COURSE 1

ACCRETION-EJECTION MODELS OF ASTROPHYSICAL JETS

RALPH E. PUDRITZ

Department of Physics and Astronomy, McMaster University, Hamilton, ON L8S 4M1, Canada

PHOTO: height 7.5cm, width 11cm

Contents

ACCRETION-EJECTION MODELS OF ASTROPHYSICAL JETS

Ralph E. Pudritz

Abstract

Astrophysical jets are almost always associated with accreting objects, be they young stellar objects or massive black holes. Their role in the evolution of accretion disks is tied to the efficiency with which hydromagnetic flows can transport angular momentum from their sources. These lectures constitute a review of the latest developments in the observation, theory, and numerical simulation of astrophysical jets. Among the most basic results in this field is the observed relation between the jet mass loss rate and the disk accretion rate $\dot{M}_w/\dot{M}_a \simeq 0.1$ which is observed in many different systems and arises in numerical simulations of all kinds. This connection was predicted to be a consequence of angular momentum extraction from the disk by magneto-centrifugal winds. These systems can be regarded as integrated accretion-ejection structures - a notion that is explored in some detail. This paper also presents new results on numerical simulations of 2D and 3D jets for a wide variety of initial magnetic configurations. Astrophysical jets are shown to have both highly collimated as well as wide-angle outflow characteristics, and they are robustly stable in 3D.

1 Introduction

Astrophysical jets are among the most fascinating and ubiquitous phenomena in astronomy. These high speed, well-collimated, episodic outflows are associated with young stellar objects (YSOs) of all masses [1], [2]; accreting stellar mass black holes or microquasars [3]; massive black holes in active galactic nuclei (AGNs) [4]; planetary nebulae [5]; and compact isolated objects such as the Crab pulsar [6]. One invariably finds that jets are associated with accretion disks around their central objects. We shall see that

---

This work is supported by a grant from the National Science & Engineering Council of Canada

the evidence strongly suggests that accretion disks are the drivers for most nonrelativistic or mildly relativistic outflows.

Jets are not merely exotic oddities in these diverse systems. Their astrophysical importance derives from the high efficiency with which they can extract and transport gravitational potential energy and angular momentum from the central engine. The evidence suggests that jets in most of these sytems are powered by accretion - the gravitational binding energy that is released by the accretion of gas onto the central object. Thus jet properties such as their terminal velocities naturally scale with the depth of the gravitational potential well of their central objects. Astrophysical jets are also highly robust structures in that they are able to propagate through inhomogenous gaseous environments (eg. clumpy gas in molecular clouds, AGNs) and out to very large physical scales.

In these lectures, I shall explore the link between accretion disks and jets in these seemingly disparate physical systems. Theoretical and numerical work strongly suggests that the simultaneous accretion of gas through a magnetized accretion disk and the ejection of a portion of it in a magnetized wind lie at the heart of the jet phenomenon. I start by discussing the key observational results on the relation between accretion disks and jets from YSOs to quasars. I then review the general theory of hydromagnetic disk winds. Finally, I review the rapidly growing body of numerical work that is contributing new insights into these processes. I also present some new simulations of jets from a wide variety of initial magnetized disks, including Blandford and Payne (1982), as well as Pelletier and Pudritz (1992). Many new results about the structure and dynamics of jets have arisen from studies of YSOs and this is reflected in the contents of this review (see also [7], [8]).

2 Observations and Basic Physics

2.1 Molecular Outflows and Jets in YSOs

Bipolar molecular outflows are the most obvious and ubiquitous sign-posts of star formation. There are now more than 200 molecular outflows known [9] and over 40 of these are associated with well collimated jets. Molecular CO outflows trace the interaction between an underlying jet and the ambient molecular cloud. The gas mass in the molecular flows ranges from $10^{-2} M_\odot$ to $200 M_\odot$ (Mon R2) while their sizes range from < 0.1 pc to 5 pc. Outflows are associated with both low-mass T-Tauri stars as well as with high mass star formation. It appears that 45% of all massive star formation regions are associated with high velocity bipolar outflows whose underlying stars correspond to mid to early B type stars [10].

Some of the best evidence for the hydromagnetic nature of the engine that drives these outflows is the well documented correlation between the thrust ($F_{CO} \simeq \dot{M}_w v_w$) of the material in the swept-up CO flow and the radiative thrust associated with bolometric luminosity of the central source ($F_{rad} \simeq L_{bol}/c$) [11]. Here $\dot{M}_w$ is the mass loss rate observed in the CO flow and v_w is the typical outflow speed.

The data show a nearly linear relation between these two quantities and that the thrust is observed to be two of orders of magnitude larger than what could be provided by a radiative drive from the central star:

$$F_{CO}/F_{rad} = 250(L_{bol}/10^3 L_{\odot})^{-0.3} \tag{2.1}$$

This empirical result excludes the driving of YSO outflows by thermal or radiative pressure alone. The mechanical luminosity of outflows, $L_{CO} \simeq (1/2)\dot{M}_w v_w^2$, is observed to be small in comparison with the luminosity of the central stars

$$L_{CO}/L_{bol} = 0.01(L_{bol}/10^3 L_{\odot})^{-0.2} \tag{2.2}$$

It is remarkable that these relations are valid over nearly six orders of magnitude in L_{bol} which strongly suggests that the outflows from both low and high mass YSOs share a similar underlying mechanism.

The velocity and morphological structure of CO outflows provide useful constraints on the physics of the underlying jet. Jets can often be traced by their shocked molecular hydrogen emission so that by comparing H_2 and CO maps of outflows one may infer how a jet interacts with the ambient medium. Two basic models for jet-driven CO outflows have had some observational success: i) jet-driven bowshocks [12] [13]; or ii) wind-driven shells that are pushed by an underlying wide-angle wind [14]. These models are compared in [15] and [2]. The former mechanism predicts that CO outflows delineate the working surfaces and bowshocks of underlying well collimated jets with the ambient medium, while the latter mechanism proposes that a wide-angle wind provides a largely undetected source of momentum that pushes on the walls of outflow cavities.

Tests of these two models have been performed by high spatial resolution OVRO observations of several molecular outflows [16]. Symmetric 2-sided H_2 jets are observed in at least one case, HH 212. They are 0.6 pc long and consist of matched knots and bow shocks along the jet which is perpendicular to an extended $C^{18}O$ disk. The CO is well aligned with the shocked jet - the tips of the CO lobes connect to the bow shocks of the jet as well as to the inner shocks. This source provides a good fit to the jet-driven bow-shock model. However, many of the other outflows in the Lee et al. [16] sample are best fit by the wide-angle wind-driven shells.

Protostellar outflows are initiated in the earliest stages of star formation and persist for as long as accretion disks are present. A quantitative measure of the prevalence of a protostellar disk in any system is obtained by measuring the system's infrared spectral energy distribution (SED) -

classified as Class 0 to Class 3. The infrared emission that is in excess of that arising from the underlying central YSO is produced by the accretion disk [17].

The most embedded sources (Class 0's) are so well hidden that even IRAS point sources are hidden at wavelengths $\lambda < 10\mu$ m [18]. Class 0 sources have infalling envelopes whose masses are comparable with those of their central objects. These are probably bona-fida protostars - objects undergoing gravitational collapse - and persist for roughly 10^4 years. Class 0's have fast CO outflows and bright submillimetre emission. The SED of a Class 0 source is essentially that of a simple black body at the temperature of the dense, obscuring envelope. Class I sources consist of an evolved protostar that is surrounded with a thick disk and a jet. Their SEDs are dominated by disk emission. This phase lasts for 10^5 year. For Class 2 objects - the so-called classical T-Tauri stars (CTTSs) - the SED is dominated by emission from the star though infrared emission from the disk is still present and one still observes jets. The characteristic lifetime for this phase is $10^6 - 10^7$ yr. Finally, the last stage - Class 3 - is called a weak lined T-Taur star (WTTS). It has no obvious associated disk or jet and lasts on the order of 10^7 yr.

There is good evidence to show that accretion disks are present in even the early Class 0 stage. Observations of one of the youngest Class 0 sources, VLA 1623 in the ρ Oph cloud, show that the source is a binary system whose disk masses are around $0.04M_\odot$ [19], [20]. Disks in other very young protostellar systems have also been found [21].

For class 0 protostars the bolometric luminosity of the central YSO arises primarily from accretion energy [18]. Class 0 sources are distinguished in having the most highly collimated flows CO outflows with speeds $v_{CO} \geq 50kms^{-1}$ [9]. They are also unusual in having mechanical luminosities comparable to the bolometric luminosity $L_{CO} \simeq (1/2)L_*$. Given that the protostellar luminosity at this early stage is dominated by accretion, one sees that the driving mechanism of the outflow must be as efficient as it could be in extracting gravitational potential energy and converting it into the mechanical energy of the outflow (the remaining 1/2 of the gravitational binding energy is released in heating the region nearest the inner edge of the accretion disk).

The underlying jet in these systems becomes amenable to direct optical observations after most of the initial core has collapsed into the disk. As an example, the well studied source DG Tau has been observed in both H_α - a good tracer of shocked gas - as well as in the forbidden line [OI] [22]. The former indicates that several bow shock structures are present and that the jet ploughs into previously ejected material. The latter diagnostic reveals the the jet moves at 200 km s^{-1} and undergoes distinct side-to-side wiggles which may be a sign that a kink mode ($m = 1$) is operative in the jet (see §4.2).

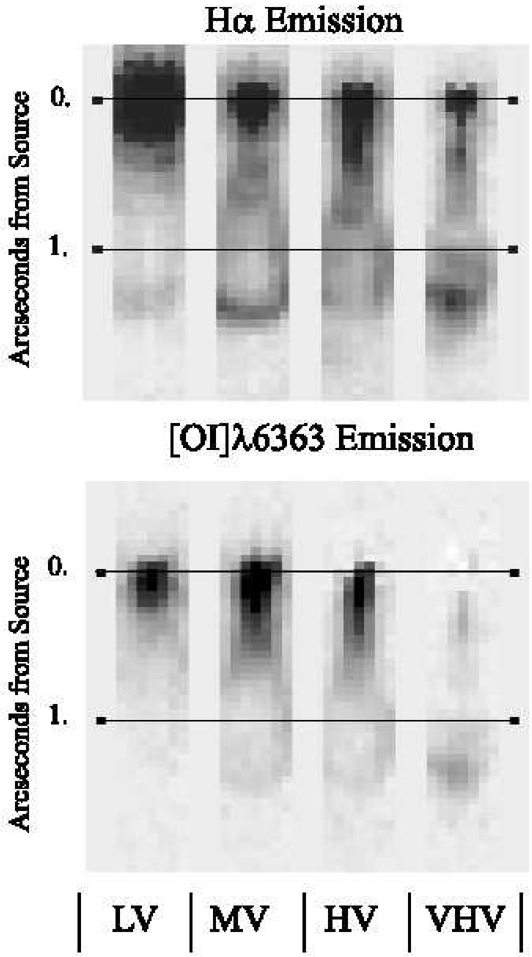

Fig. 1. Synthetic images of the DG Tau outflow in H_α and [OI] derived from 7 overlapping long-slit positions offset in the transverse direction to the flow. Courtesy of Bacciotti et al [23]

Figure 1 shows high resolution images of H_α and [OI] emission in the DG Tau jet taken in various velocity ranges from $50-450$ km s^{-1} in 125 km s^{-1} wide velocity bins [23]. The top image shows two distinct bow shocks in the mid velocity range (MV). Its density increases towards the star and axis. One also sees that there is a continuous variation in the velocity of the jet, the highest (VHV) being nearest the jet axis, and the lowest farther away. The very high speed gas (VHV) gas is the most collimated and is denser than the lower speed gas. The lower speed flow is farther from the axis and appears to broaden out and become less collimated with increasing radius in the jet. The jet can be traced to within 15 AU (0.1") of the central source. These remarkable images correspond well to the theory and simulations of disk winds (see §3.1 and §4.1 respectively). While earlier papers suggested that jets may have two distinct velocity components (fast and high collimated, versus slower and wide-angled components; [24], these data suggest a continuously varying velocity structure.

There is also good evidence that this flow is rotating clockwise when viewed from the flow towards the source [25]. The rotation speed is 6 - 15 km s^{-1}, depending on the position in the flow within 110 AU from the source. These authors find agreement between these measured rotation speeds with those expected in a centrifugally driven hydromagnetic wind. Using the scalings for disk wind speeds and angular momentum transport rates outlined in §3.1 and §3.2, this outflow is estimated to be carrying up to 60 % of the necessary angular momentum loss from the disk at its footpoint.

HST observations provide direct information about the structure and dynamics of the underlying (optical) jets from YSOs - HH30 being one of the most outstanding examples. This jet is associated with a flared, optically thick disk with a diameter of about 450 AU. The jet is resolved with a FWHM at the base of 25 AU. Jet structure is resolved down to 0.1" scales, proper motions are 100-300 km s^{-1}, and knots in the jet are generated at the rate of 0.4 new knots per year [26]. Jet collimation occurs within a cone of 3^o, within 30 AU of the source. Moreover, the transverse velocities of the knots is consistent with zero.

The mechanism of jet collimation can be constrained by observing the opening angle of a jet as a function of its distance from the source. As an example, the jet in HH30 has a 3^o opening angle between 0.5" and 5" from the source and is only 1.9^0 between 2.5" to 75". Given that any inertial confinement would be expected to diminish with distance from the source, this argues that the jet may be collimated by magnetic forces.

Finally, jets are highly time-dependent phenomena. This has implications for how we attempt to model them. In addition to the appearance of knots on short time scales (on the order of months), jets are dominated by a series of large bow-shocks. The dynamical time scales associated with these bow shocks indicates that jets are episodic on time scales of 10^3 years. This time scale is similar to the time scale for the recurrance of FU Ori outbursts in disks around TTSs as discussed below [27].

2.2 *YSO Accretion Disks: Links to Jets*

Millimetre [28], [29] as well as near IR surveys [30] showed that 50 % of YSOs harbour accretion disks and that the median disk mass (modulo uncertainties about dust emission properties) is several times $10^{-2}M_{\odot}$. These disk masses are comparable to the minimum mass solar nebular models necessary to form the solar system. The HST images of silhouette disks in the Orion nebula provide striking proof that accretion disks are an essential part of star formation.

Surveys for optical and near IR jets in the Taurus region reveal that jet activity wanes with the gradual disappearance of disks - 60 % of Class I objects have jets as compared with 10 % in Class IIs, and none in Class III objects [31]. Observational connections between the mass of circumstellar disks and molecular outflows [32] shows that sources with well developed outflows had 20 times the (1.3) millimeter flux of sources that did not have flows. This also suggests that accretion rates ($\dot{M}_a$) through disks may be higher in the earlier phases of disk evolution than later.

There is a strong correlation between the observed mass accretion rate through protostellar disks and the mass loss rates carried by their associated jets. Optical jets associated with TTS have typical mass loss rates that are consistently about a tenth of the underlying disk accretion rate. The jet in HH30, as an example, has a mass outflow rate as determined from emission line diagnostics of $5 \times 10^{-10} M_{\odot}$ yr^{-1}. The total jet mass loss rate is a factor of ten times greater than this. This in turn is 10% of the material that is accreting through the disk; $\dot{M}_a \simeq 5 \times 10^{-8} M_{\odot}$ yr^{-1}. Hartmann and Calvet [33] found, for a sample of 31 TTSs, jet mass loss rates calculated from the forbidden lines in the range $3 \times 10^{-7} < \dot{M}_j < 10^{-10} M_{\odot}$ yr^{-1} with a median value of $10^{-9} M_{\odot}$ yr^{-1} (eg. review [34], and Calvet these Proceedings). These mass loss rates are a tenth of the underlying disk accretion rate in the system;

$$\dot{M}_j / \dot{M}_a \simeq 0.1. \tag{2.3}$$

A class of YSOs with an especially high accretion rates are known as FU Ori systems ([27]). These systems are suspected to be accretion disks around TTSs that undergo disk instability leading to high accretion rates and disk temperatures. Jets associated with FU Ori bursts are particularly easy to study and have provided some excellent tests for theoretical models of jets. Fu Ori luminosities range from 200 - 500 $L_{\odot}$ while that of a typical TTS is only $\simeq 1$ $L_{\odot}$. The emission in these systems is completely dominated by the disk and temperature reach $T \simeq 7,000^o$ K in the inner regions. The wind mass-loss rates in FU Ori jets are nearly 4 orders of magnitude greater than in the TTS phase, at $\dot{M}_w \simeq 10^{-5} M_{\odot}$ yr^{-1}. Even in this phase, however, the ratio of wind mass loss rate to disk accretion rate is again

$\dot{M}_w/\dot{M}_a \simeq 0.1$ [33]. The next chapter provides a theoretical explanation of this robust result.

One can probe regions near the base of the jet, through a well-chosen set of absorption lines, to determine whether or not accretion disks accelerate these outflows (see Calvet - these Proceedings). Calvet et al ([35]) searched for this connection by choosing two types of metallic absorption lines; weak lines which probe the region deep in the disk atmosphere close to its surface (where one expects to see double-peaked lines due to the Kepler rotation), and stronger absorption lines which form in the upper disk atmosphere where the outflow speed is expected to approach the local escape speed. Their observations clearly show that double peaked weak lines which dominate in the high column depth region near the disk surface give way to single peaked strong lines farther from the disk. This strongly implicates accretion disks as a central component of the driving engine.

2.3 Magnetic Fields: from Molecular Clouds to Disks Around YSOs

There is abundant evidence that magnetic fields are important on a variety of spatial scales in molecular clouds. Zeeman measurements on the VLA and GBT of a sample of 27 clouds [36] find that magnetic fields dominate the thermal energy of the gas at densities $\geq 10^3$ cm^{-3} ($\beta = P_{gas}/P_{mag} \simeq 0.04$). The magnetic field energy density is comparable to gravitational energy densities as predicted by the virial theorem; $M \simeq (1/2)W_{grav}$.

The structure of the magnetic field in dense gas is best inferred by sub mm polarimetry. At these wavelengths, dust emission predominates over scattering. Spinning dust grains are aligned by the magnetic field with their long axes perpendicular to the magnetic field line so that sub mm polarimetry traces the structure of cloud's magnetic field. The observations are surprising - relatively well ordered fields are seen down to scales 0.04 pc [37], [38], [39]. The data is well fit by a theoretical model for filamentary molecular clouds in which helical field lines wrap around the filaments [40], [41].

There is some evidence for the existence of strong, ordered magnetic fields that are associated with jets. A radio map of T-Tau at 6 cm [42] shows that two lobes of opposite helicity, circularly polarized emission straddle the central star. The emission is likely to be gyrosynchotron from mildly relativistic electrons ($\gamma \simeq 2-3$). The field strength deduced is $B_j \geq$ several Gauss at a distance of 10 - 20 AU from the source. The associated magnetic pressure $B_j^2/8\pi = 3.6 \times 10^{-1}(B/3G)^2$ dyne is large compared to the ram pressure of the jet; $\rho_j v_j^2 \simeq 0.67 \times 10^{-3}(n_j/10^4\mathrm{cm}^{-3})(v_j/200\mathrm{kms}^{-1})^2$ dyne. The structure of the field is not determined by these observations, One anticipates however that since the toroidal field falls probably falls off less steeply than a poloidal field in the jet ($B_\phi \propto r^{-1}$), one may be probing a strong toroidal field at these scales. Jet collimation will arise from the associated hoop stress (see §3.3).

It is very difficult to obtain direct evidence for magnetic fields that are associated with the accretion disks at this point in time. Nevertheless, Zeeman observations of an $H30\alpha$ maser recombination lines at 1.3mm have found a field strength of 22 mG at 40AU [43]. This field strength is below equipartition strength with the gas pressure of a standard disk at these radii, but is still significant. Finally, the meteoritic evidence shows that a magnetic field strength approaching 1 Gauss (at 3 AU) must have been present in the solar nebula [44].

A prerequisite for any hydromagnetic flow phenomenon is that the fluid be a good conductor. For the dense regions that can occur in protostellar accretion disks, however, this is not generally true. Molecular clouds are heated by the flux of cosmic rays through them. More significantly, the bulk of the lower density molecular gas in clouds is probably ionized by X-rays from YSOs of all classes (with the possible exception of Class 0's). YSOs are copious X-ray producers with X-ray energies 2-5 keV (eg. [45], [46], Montmerle these Proceedings). At 5 kev, X-rays penetrate material down to a visual extinction of $A_v \simeq 100$, which corresponds to a column density of up to 30 g cm^{-2}. This provides reasonable coupling of magnetic fields within the bulk of a molecular cloud's volume. However, penetration depth of X-rays is far less than the column density of the minimum mass solar nebula, which has typically $\Sigma_{min}(1AU) \simeq 1500$ g cm^{-2}. The interiors of these disks can only be ionized by cosmic rays (see §2.6).

2.4 The Role of Jets and Accretion Disks in Star Formation

Star formation involves the collapse of an initially slightly rotating molecular cloud core into an embryonic protostellar core and a surrounding accretion disk. Most of the material that forms the star probably flows through the accretion disk first so the question of how angular momentum is removed from disks is pivotal to the theory of star formation. The energy that is liberated as gas accretes through a disk depends on the depth of the gravitational potential well produced by the central object, as well as the disk accretion rate $\dot{M}_a$. Any ordered magnetic field that threads through a spinning object - be it a disk or a star - exerts a torque upon it. This torque can extract the object's angular momentum and transport it away from the disk in a wind. The gravitational binding energy that is released during accretion appears as the mechanical energy of the outflow. Other competing torques that drive angular momentum transport in disks without driving a wind are due to spiral waves and MHD turbulence. Although it has been suggested that outflows and jets might help to determine the mass of a star by ejecting the material in the infalling envelope, it is difficult to see how the well collimated jets in the Class 0 phase have the necessary cross-sectional area to do the job.

Numerical simulations of the collapse of finite mass, non-singular cores, find that the infall rate varies with time with high initial rates giving way to slower infall rates as the remaining remnants of an initial core envelope are accreted onto the central object (eg. [47], [48]). Gravitational collapse of the molecular cloud core in which a star formsfeeds the disk accretion and ultimately, jet activity. One would therefore expect this evolution of the infall rate to be mirrored in the changing strength of the outflows. This appears to happen - outflow activity is diminished in going from Class 0 to Class I sources. The former have thrusts that are a factor of 100 larger than the latter. Measurements of the diminishing thrusts for 45 young YSOs suggest that the accretion rate in the disk decreases with time [49]. This can be seen by writing the observed thrust carried by the CO outflow as $F_{CO} = f_{ent}(\dot{M}_w/\dot{M}_a)\dot{M}_a v_w$ where $\dot{M}_a$ is the accretion rate through the disk. Theoretical arguments, which will be discussed in the next section, suggest that the accretion ratio, $\dot{M}_w/\dot{M}_a \simeq 0.1$ may remain nearly constant through various phases of disk evolution ([50], [51]), so that outflow evolution reflects the diminuation of accretion rates from $\dot{M}_a \simeq 10^{-5}$ to 10^{-7} $M_\odot$ yr^{-1}.

The disk lifetimes for low mass TTS - measured by fitting isochrones to central TTS - is $\simeq 10^6$ yr. This implies that roughly $10^{-2}M_\odot$ accretes onto the YSO in these later phases of TTS evolution. If TTSs typically undergo the transition to FU Ori behaviour, and these outbursts have a duration of order 2000 years (as is suggested by time scale associated with jet outbursts) then most of a star's mass may be accreted in 5-10 of these outbursts within disks [52]. Thus, the accretion rates that are mediated by jet outflows may be the predominant mode of building a central star.

2.5 Relativistic Systems: Microquasars, Quasars, and X-ray pulsars

The link between jets and disks is observed in many relativistic systems as well (see Sunyaev, these Proceedings). There are 200 galactic X-ray binaries systems known. X-ray emission arises from the inner parts of accretion disk around a compact primary - either a neutron star or black hole [53]. Of this population only 10 % are radio loud, and 10 have relativistic jets with $v > 0.1c$ [3]. The proof that these are relativistic jets comes from the superluminal motion of discrete knots that one sees in several of these sources - most famously GRS 1915+105 [54]. The presence of two IRAS sources along the jet axis indicates its interaction with the surrounding environment. The jets associated with stellar mass black holes are like those seen in quasars - with the considerable advantage that all of the time scales in the former are shorter by the ratio of the orbital times at their respective Schwarzschild radii $\propto (M_{stellar}/M_{quasar}) \simeq 10^{-7}$.

Jets and accretion disks also appear to be well correlated in the context of quasars such as NGC4258. Here, VLBI observations reveal a set of spatially resolved water masers that extend from 0.13 - 0.25 pc from the central object. The radial velocities of the disk-like spatial distribution of these masers fall on a Keplerian rotation curve, implying a central black hole mass of $\simeq 3.5 \times 10^7 M_\odot$ [55]. Perpendicular to this flared disk, one can discern an extended structure which may be the base of the relativistic jet that is observed on kpc scales. This may represent the shocks that may be seen in relativistic flows [56].

Why is the jet frequency apparently so low in microquasars and quasars (perhaps $\simeq 10\%$) and yet so high YSO disk/jet systems? Accretion disks around black holes are expected to be geometrically thick and to have a very different underlying dynamics (eg. review [57]. In the so-called ADAF solutions, most of the gravitational energy release goes into heating the tenuous gas of the disk which, it is proposed, is then swallowed by the black hole without radiating very much [58]. On the other hand, there are good arguments to suggest that such disks ought to have winds that carry off this hot, tenuous gas before it has the chance of being so devoured - the so-called ADIOS solutions [59]. In this latter case, relativistic jets may be as common as their YSO counterparts, but they are simply too tenuous to be readily detected.

A beautiful example of a jet from a compact object that does not have an associated accretion disk is the Crab pulsar. The theory of magnetized winds was originally developed to explain the braking of magnetized stars (see next section). Sufficiently rapidly rotating isolated objects such as pulsars therefore, ought to show outflows that are unrelated to accretion disks, but that are nevertheless collimated. The X-ray emission from the Crab was recently mapped using the Chandra observatory [6]. The X-ray emission is observed to be more compact than that from the optical nebula (about 40 % as large). The data show both an X-ray torus as well as a knotted jet and counterjet that is perpendicular to the semi-major axis of the torus ($\simeq 0.37$ pc - with a semi-minor axis of 0.17 pc). The X-ray jet emission indicates continuous emssion from highly relativistic particles that are flowing parallel to the pulsar magnetic axis. Axisymmetric solutions for outflows from rapidly rotating magnetized stars show that such outflows can become highly collimated along their rotation axes [60]. In such situations, it is the spin energy of the rapidly rotating neutron star that ultimately powers the jet.

2.6 Magnetized Accretion Disks: General Physical Processes

What general characteristics are expected of a magnetized disk and its jet? In particular, how are magnetized disks heated - and why do they drive off jets? Is a disk corona required to initiate such a wind (as in the solar wind)? Given that the only astrophysical MHD laboratory that we can directly observe is the Sun, what general physical processes seen on the Sun will be important for understanding disk-jet systems?

The activity of the solar corona provides some important insights. Three major mechanisms have been proposed for heating the solar corona: (i) heating by current dissipation during magnetic reconnection of the loops, (ii) damping of Alfvén waves, and (iii) MHD turbulence. Observations from two X-ray imaging satellites, Yohko and Soho, as well as the imaging ultrviolet satellite TRACE resolve the physics of the solar corona on physical scales ranging from $60R_{\odot}$ down to $5 \times 10^{-4} R_{\odot}$. The magnetic field on the Sun consists of a heirarchy of magnetic loops in which magnetic reconnection and flares occur. Flares have energies ranging over 7 decades in magnitude down to so-called nanoflares which release $\geq 10^{24} - 10^{27}$ ergs. The contribution of flare energy can be ascertained by measuring the flare frequency distribution. By combining the hard and soft X-ray data, as well as the EUV emission from 281 nanoflares, Aschwanden et al. [61] find the power-law relation $N(E) \simeq 10^{-46}(E/10^{24} erg)^{-1.8}$ s^{-1} cm^{-2} erg^{-1}. This result shows that there is insufficient power of nanoflares to heat the solar corona. Non-luminous energy carriers such as waves may provide the dominant mode of heating the solar corona.

These solar results may be relevant to accretion disks. Accretion disk models typically assume that turbulent heating occurs in disks, although there is not much known about energy deposition in a disk corona. Thin accretion disks are highly sheared flows. Magnetic loops cannot have footpoints that are widely separated in disk radius since the dominant Kepler shear would stretch these out leading to reconnection. Magnetic buoyancy would ensure that a forest of loops would protrude from the disk surface and that shear would orient these in largely toroidal direction. MHD turbulence in the body of the disk is the expected end-state of the operation of the magneto-rotational (MRI) instability ([62], [63], Blaes - these proceedings). This instability results in the exponential growth of magnetic field on the Oort dynamical time-scale, and saturation occurs when the Alfvén velocity $v_A \leq c_s$ in the disk.

Accretion disks and their coronae could be heated by a combination of flares, an inverse cascade of turbulent (MHD) energy, or by dissipation of Alfvén waves. It is still unknown as to how much of the gravitational potential energy that is released locally from accretion would actually be dissipated within the body of the disk as compared to dumping it in a corona. Global simulations of the MRI instability in thin disks show that considerable wave energy flows into a disk corona and where it is damped in shocks ([64] - see §5).

The production and collimation jets may require that accretion disks be threaded by an ordered magnetic field. What is the source of this field? The two possibilities are that the field pervades the larger-scale medium (eg. protostellar cloud core) and is advected along with the material that forms the accretion disk - or - that the field it is generated in situ by local dynamo action or MRI instability.

Consider the first scenario. The dynamics of a mean field in a disk with a turbulent viscosity ν_T and magnetic diffusivity η_T is controlled by the magnetic Prandtl number defined as their ratio. We follow the convention of Lubow et al. [65] and write it as $Pr_m \equiv \eta_T/\nu_T$. In the limit of small Prandtl number ($Pr_m << 1$) viscosity dominates field slippage and the field is dragged inwards by the radial flow ($v_r \propto \nu_T$). In the opposite limit, $Pr_m >> 1$, the large magnetic diffusivity that arises from poor conductivity of the gas leads to outward slippage of the field which dominates over its inward advection by the accretion flow. Stationary solutions in idealized thin disk models show that the basic governing parameter for field evolution is $D \equiv (H/r)Pr_m$ where $H(r)$ is the disk pressure scale height. The radial inflow speed is $v_r = -3\nu_T/2r$ and the ratio of the radial to vertical components of the disk field is given by $B_r/B_z = tan^{-1}\theta \simeq D^{-1}$ where θ is the opening angle of the field with respect to the vertical axis (Lubow et al 1994). The opening angle of the field is very important for the dynamics of hydromagnetic winds, so this result shows that disk physics and outflow dynamics are intimately coupled with one another. Centrifugally driven outflows are favoured when $D \simeq 1$.

In the second scenario, magnetic fields are generated in situ. The MRI instabiltiy may feed local dynamo action ([66], [67]) wherein the energy in the sheared Kepler flow is converted into magnetic energy. While traditional dynamo actions required helical turbulence in order to produce a poloidal field from a toroidal one as an example, Balbus and Hawley emphasize that the MRI instability does not require helical turbulence. It is also interesting to note that the MRI instability can also be tapped by radial global modes in a disk which grow at somewhat slower but still significant rates [68]. Global simulations of disk confirm that these global modes are generated [69].

All of the discussion on accretion-ejection structures has assumed that accretion disks are good conductors and that therefore the magnetic field is well coupled to the gas. While the disks in FU Ori systems, quasars and microquasars are hot enough to guarantee this, the dense disks around TTSs may not be well coupled throughout their volume. Turbulent transport of angular momentum requires that the MRI instability be operative. In a resistive disk, there will be some scale λ whose growth rate through MRI instability ($\simeq v_A/\lambda$) is just balanced by the dissipation rate (η/λ^2) prescribed by the microphysical magnetic diffusivity η. Thus, magnetic viscosity will be completely damped out on physical scales whose magnetic Reynold's numbers are $Re_m \equiv v_A\lambda/\eta \leq 1$ [70]. The magnetic diffusivity of the gas depends on its degree of ionization, such that $\eta = 1.5 \times 10^{-12} T_{500}^{1/4} \zeta_{-17}^{-1/2} n_{H,13}^{-1/2}$ cm^{-2} s^{-1} where the temperature is in units of 500 K, the cosmic ray ionization rate is in units of particles per 10^{17} sec, and the density is in units of 10^{13} cm^{-3}. The resulting "dead-zone" (where material is decoupled from the field) for a protostellar accretion disk may extend out to several A.U. and leave only a relatively thin well-coupled surface layer along which accretion flow can still occur. This zone also has significant consequences for planet formation [71].

Having discussed the observational and physical underpinnings of jets from accretion disks, we now review some of the essentials of the large body of theoretical work on the physics of jet production.

3 Theoretical Models

3.1 Axisymmetric Hydromagnetic Winds: Conservation Laws

The theory of hydromagnetic winds originated with the early work on winds from rotating magnetized stars [72], [73]. These papers developed 1-D, axisymmetric models of hydromagnetic flows from rotating stars. They showed that a centrifugally driven, stellar wind could efficiently transport stellar angular momentum, leading to the spin down of the central star. The application of this idea to self-similar accretion disks was carried out in the seminal paper by Blandford & Payne (BP) [74].

Consider the simplest possible description of a magnetized gas, rotating gas threaded by a large-scale field. The equations of stationary, ideal MHD are the conservation of mass (continuity equation); the equation of motion with conducting gas of density ρ undergoing gas pressure (p), gravitational (from the central object whose gravitational potential is ϕ), as well as the Lorentz force (from the field $\mathbf{B}$); the induction equation for the evolution of the magnetic field in the moving fluid; as well as the conservation of magnetic flux. These equations were written down by Chandrasekhar, Mestel, and many others;

$$\nabla.(\rho\mathbf{v}) = 0 \tag{3.1}$$

$$\rho\mathbf{v}.\nabla\mathbf{v} = -\nabla p - \rho\nabla\phi + \frac{1}{4\pi}(\nabla\times\mathbf{B})\times\mathbf{B} \tag{3.2}$$

$$\nabla\times(\mathbf{v}\times\mathbf{B}) = 0 \tag{3.3}$$

$$\nabla.\mathbf{B} = 0 \tag{3.4}$$

It is convenient to decompose all magnetic fields and velocity fields into poloidal and toroidal field components $\mathbf{B} = \mathbf{B_p} + B_\phi\hat{\mathbf{e}}_\phi$ and $\mathbf{v} = \mathbf{v_p} + v_\phi\hat{\mathbf{e}}_\phi$.

The solution of the induction equation is particularly simple;

$$\mathbf{v_p}\times\mathbf{B_p} = \nabla\psi \tag{3.5}$$

where ψ is akin to an "electrostatic" potential. This solution has two important ramifications. The first arises from the toroidal component of the equation which states that $\partial\psi/\partial\phi = 0$; a simple consequence of axisymmetry. Therefore, the poloidal velocity in axisymmetric and stationary flows must be oriented along magnetic field lines, ie, parallel to the poloidal field component $\mathbf{v_p}||\mathbf{B_p}$. Another obvious consequence of the induction equation follows by taking the dot product of it with $\mathbf{B}$, which gives $\mathbf{B_p}.\nabla\psi = 0$. Thus, ψ is a constant along field lines and is nothing other than the (poloidal) magnetic flux.

Let us turn now to the equations (3.1) and (3.4) that express the conservation of mass and magnetic flux. By comparing the form of these two equations, we see that the poloidal field and the poloidal mass flux along the field line must be proportional to one another along a field line. Defining a function k that is a constant along a magnetic field line and which we will call the "mass load" of the wind, then;

$$\rho\mathbf{v_p} = k\mathbf{B_p} \tag{3.6}$$

This mass load function can be revealingly cast by noting that the wind mass loss rate passing through an annular section of the flow of area dA through the flow is $d\dot{M}_w = \rho v_p dA$, while the amount of poloidal magnetic flux through this same annulus is $d\Phi = B_p dA$. Thus, the mass load per unit time, per unit magnetic flux of the wind that is preserved along each streamline along the flow emanating from the rotor (a disk in this case) is

$$k = \frac{\rho v_p}{B_p} = \frac{d\dot{M}_w}{d\Phi} \tag{3.7}$$

The mass load is determined by the physics of the underlying rotor, which is its source. As we whall see, this source boundary condition plays an important role in the physics of the resulting magnetized wind.

We can extract additional information from the induction equation by examining its poloidal component; $\mathbf{v_p} \times \mathbf{B}_\phi + \mathbf{v}_\phi \times \mathbf{B_p} = \nabla\psi|_\mathbf{p}$. This may be simplified by using the relation between v_p and B_p, to find that $\psi = \Omega - (kB_\phi/\rho)$ where $\Omega(r)$ is the local angular velocity of the gas at any point in the flow. In order to evaluate ψ, note that at the mid-plane of the disk, the toroidal field *must* vanish by symmetry. Thus $\psi = \Omega_o$, the angular velocity of the disk at mid-plane. Thus, one has found the relation between the toroidal field and the angular velocity in a rotating flow;

$$B_\phi = \frac{\rho r}{k}(\Omega - \Omega_o). \tag{3.8}$$

This result has an interesting consequence for jet collimation - the larger the value of k along a field line, the smaller is the value of the toroidal field. This is an inertial effect; it implies that jets that have low density with respect to the magnetic flux that threads them will have stronger toroidal fields and will hence be more easily collimated by the resulting hoop stress.

Consider the **angular momentum equation** for axisymmetric flows. This is described by the ϕ component of equation (3.2), which yields;

$$\rho \mathbf{v_p}.\nabla(r v_\phi) = \frac{\mathbf{B_p}}{4\pi}.\nabla(r B_\phi) \tag{3.9}$$

Let us apply this equation to two different situations - (i) the transport of angular momentum along a field line and (ii) the transport of angular momentum out of a disk, by an outflow (which is analyzed in the following subsection).

By applying equation (3.6) to equation (3.9) we find that angular momentum flow along a field line reduces to the statement that

$$\mathbf{B_p}.\nabla(r v_\phi - \frac{r B_\phi}{4\pi k}) = 0 \tag{3.10}$$

This equation says that there is a quantity,

$$l = r v_\phi - \frac{r B_\phi}{4\pi k}, \tag{3.11}$$

which is a constant along a field-line in the flow. This is just the total angular momentum per unit mass. The form for l reveals that the total angular momentum is carried by both the rotating gas (first term) as well by the twisted field (second term).

The solution for the toroidal components of the outflow velocity may now be found by eliminating the toroidal field between equations (3.8) and (3.11);

$$r v_\phi = \frac{l m^2 - r^2 \Omega_o}{m^2 - 1} \tag{3.12}$$

where the so-called Alfvén Mach number of the flow is $m^2 = v_p^2/v_A^2$ and $v_A = B_p/\sqrt{(4\pi\rho)}$ is the Alfvén speed of the flow. The Alfvén surface is that point $r = r_A$ at each field line in the wind where $m = 1$. The flow may be regarded as kept in co-rotation with the rotor until this point is reached.

We see that in order that no spurious singular behaviour occur at the Alfvén surface (m=1), the value of the specific angular momentum is then fixed;

$$l(a) = \Omega_o r_A^2 \tag{3.13}$$

For a field line starting at a point r_o on the rotor (disk in our case), the Alfvén radius is $r_A(r_o)$ and constitutes a lever arm for the flow. The true critical points of the outflow are where speed v_p equals the speed of the slow and fast magnetosonic modes in the flow (at the so-call SM and FM surfaces). The Alfvén point is not a true critical point in the flow; flow passing steadily through SM and FM surfaces must go through the Alfvén surface.

Finally, a generalized version of Bernoulli's theorem may be derived by taking the dot product of the equation of motion with $\mathbf{B_p}$. Thus, there is a specific energy $E(a)$ that is a constant along field lines, given by (eg. Pelletier and Pudritz (PP92) [51];

$$E(a) = \frac{1}{2}(v_p^2 + \Omega^2 r^2) + \phi + h + \Omega_o(\Omega_o r_A^2 - \Omega r^2) \tag{3.14}$$

The terminal speed $v_p = v_\infty$ is such that the gravitational potential and rotational energy of the flow are negligible. For cold flows, the pressure may also be ignored. It follows that

$$v_\infty \simeq 2^{1/2}\Omega_o r_A \tag{3.15}$$

which is a result first obtained by Michel [75] for 1-D flows. The important point regarding outflow speeds from disks is that $v_\infty/\Omega_o r_o = 2^{1/2} r_A/r_o$; the poloidally directed flow is larger than the rotor speed by a factor $r_A(r_o)/r_o$ which is just the lever arm of the magnetic wind torque on the disk.

3.2 MHD Wind Torques on Disks: Jets as the Mechanical Manifestation of Accretion Power

Let us now carry out our second application of the angular momentum equation (3.9), this time to find the torque that is exerted upon a thin accretion disk by an external field $\mathbf{B}$. Any vertical flow in the thin disk is negligible so only the v_r contribution matters, and the rotation speed v_ϕ is the Kepler speed if disks are thin. On the right hand side, both the radial and vertical magnetic contributions come into play; thus

$$\rho v_r \frac{\partial(r_o v_\phi)}{\partial r_o} = \frac{B_r}{r_o}\frac{\partial(r_o B_\phi)}{\partial r_o} + B_z \frac{\partial B_\phi}{\partial z} \tag{3.16}$$

One sees that specific angular momentum being stripped out of the radial inward accretion flow is due to the action of two types of magnetic torque. The first term on the RHS represents radial outward transport of angular momentum due to the radial shear of the toroidal field, while the second term is vertical tranport due to the vertical shear of the toroidal field as it threads the disk. In a thin disk, and for a typical field opening angle, the second term will dominate. Note that the second term vanishes at the disk mid-plane because symmetry considerations force $B_r = 0$ on the mid-plane. We then vertically integrate the resulting equation, noting that the disk accretion rate is $\dot{M}_a = -2\pi\Sigma v_r r_o$. The result is the angular momentum equation for the accretion disk under the action of an external magnetic torque;

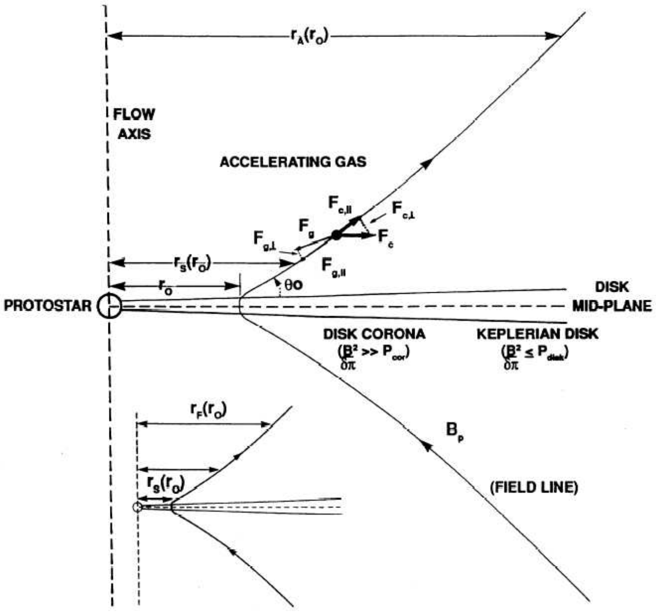

Fig. 2. Geometry and dynamics of a disk wind from a thin accretion disk. The three critical points corresponding to the slow magnetosonic r_S, Alfvénic, r_A, and fast magnetosonic r_F conditions in the jet are shown. From Pelletier & Pudritz [51].

$$\dot{M}_a \frac{d(r_o v_o)}{dr_o} = -r_o^2 B_\phi B_z|_{r_o,H} \tag{3.17}$$

This result shows that angular momentum is extracted out of disks threaded by magnetic fields. It is ultimately attached to either toroisional Alfvén waves, or, with magnetic field lines inclined by more than 30^o from the vertical, to a wind. By solving for $rB_\phi = k(rv_\phi - l)$ and relations (3.7 and (3.13) for k and l the above disk angular momentum equation (3.17) can be cast into its most fundamental form;

$$\dot{M}_a \frac{d(\Omega_o r_o^2)}{dr_o} = \frac{d\dot{M}_w}{dr_o} \Omega_o r_A^2.(1 - (r_o/r_A)^2) \tag{3.18}$$

This equation shows that there is a crucial link between the mass outflow in the wind, and the mass accretion rate through the disk;

$$\dot{M}_a = (r_A/r_o)^2 \dot{M}_w \tag{3.19}$$

This result simply states that the rate at which the disk loses angular momentum, $\dot{J}_d = \dot{M}_a \Omega_o r_o^2$, is exactly the rate that is carried away by the wind, $\dot{J}_w = \dot{M}_w \Omega_o r_A^2$. The crucial point about the magnetic fields in any MHD wind is that they force gas to co-rotate with the rotor out to a distance of the order r_A.

The value of the Alfvén lever arm $r_A/r_o \simeq 3$ for most theoretical and numerical models that we are aware of, so that one finds $\dot{M}_w/\dot{M}_a \simeq 0.1$. Thus, the observed link between accretion and outflow has a natural explanation in the context of disk wind theory. This can be traced to the fact that magnetic wind torques have lever arms that are *external* to the disk, and therefore potentially very large. This is quite distinct from the scaling that arises from viscous torques which have lever arms that are no more than αH where α is the S-S parameter for the torque (the value is about 10^{-2} in the MHD simulations of Balbus-Hawley turbulence). The ratio of an MHD disk wind torque to a viscous disk torque may be written as $(B_z^2/4\pi P).(r_A/\alpha H)$ [51] which shows that even if the magnetic energy density within a disk is far less than the gas pressure P, its lever arm is still sufficiently large to beat viscous stresses in the competition to transport disk angular momentum. The only natural competitor for magnetic wind torques upon disks may be spiral waves which also have long lever arms.

We may now connect this theoretical analysis with the observations of momentum and energy transport in the molecular outflows reviewed in §2.1. First we may use equation (3.18) to calculate the total mechanical energy that is carried by the jet;

$$L_w = \frac{1}{2}\int_{r_i}^{r_j} d\dot{M}_w v_\infty^2 \simeq \frac{1}{2}\frac{GM_*\dot{M}_a}{r_i}[1-(r_i/r_j)^2] \simeq \frac{1}{2}L_{acc}. \qquad (3.20)$$

This results states that the wind luminosity taps the gravitational energy release through accretion in the gravitational potential of the central object. The last equality - which pertains to the case in which all of a protostar's energy release is still due to accretion - matches the observations of jet luminosity of the class 0 objects (see §2.1).

We may also calculate the total momentum flux (thrust) carried by a jet launched from an accretion disk. For simplicity, assume that the Alvén radius of flow along a field line whose footpoint is located at r_o obeys a power law scaling $r_A(r_o)/r_o \propto r_o^{-\beta}$. The thrust is then

$$\frac{F_w}{L_{bol}/c} = \frac{c}{L_{bol}}.\int_{r_i}^{r_j} d\dot{M}_w v_\infty = f(\beta)\frac{r_i}{r_{A,i}}\frac{c}{v_{esc,i}}\frac{L_w}{L_{bol}} \qquad (3.21)$$

where $f(\beta) \equiv (4/[1+2\beta])$ and the index i denotes the inner disk radius, and $v_{esc,i}$ is the escape speed from r_i. This result accounts for the fact that the observed thrust of the CO is larger than L_{bol}/c since $c/v_{esc,i} \simeq 10^3$ while $L_w/L_{bol} \simeq 10^{-2}$. It also shows that the thrust scales with L_w/L_{bol} and will therefore have the largest value for the largest values of the luminosity ratio - which occurs during the Class 0 stage.

3.3 Force-Balance in Jets; the Mechanism of Jet Collimation

The most stiking observational feature of jets is that they remain so well collimated over many decades in physical scales as they work their way through inhomogenous media far from their source. How is this accomplished?

In the standard picture of hydromagnetic winds, collimation of an outflow occurs because of the increasing toroidal magnetic field in the flow as one moves through its various critical points. From equation (3.8) one deduces that at the Alfvén surface $B_\phi \simeq B_p$, while in the far field (assuming that $r_j >> r_A$) this ratio is of the order $B_\phi/B_p \simeq r/r_A$. Therefore, collimation can in principle be achieved by the tension force associated with the toroidal field which leads to a radially inwards directed component of the Lorentz force (or "z-pinch"); $F_{Lorentz,z} \simeq J_z B_\phi$.

The detailed radial structure of the outflow is found from the condition of force balance perpendicular to the field lines in the flow, which is known as the Grad-Shafranov equation. This is one of the most complicated non-linear equations in theoretical physics (see contributions by Heyvaerts and Beskin - these Proceedings). No general solutions are known [76]. Because of the mathematical difficulties, analytic studies have been dominated by simplified approaches which focus mainly on finding stationary, self-similar solutions of the flow ([74], [77], [78], [79], [80]), or on analyzing the asymptotic limits of the general equations ([81], [51]).

Heyvaerts and Norman [81] show that two types of solution are present depending upon the asymptotic behaviour of the total current intensity $I = 2\pi \int_0^r J_z(r', z')dr' = (c/2)rB_\phi \propto r^2 \rho \Omega_o$ where, $\mathbf{J} = (c/4\pi)\nabla \times B$ is the current density. In the limit that $I \to 0$ as $r \to \infty$, then the field lines are paraboloids which fill space. On the other hand, if the current is finite in this limit, then the flow is collimated to cylinders. The character of the flow therefore depends upon the boundary conditions on the disk.

Self-similar solutions have provided considerable insight into the physics of disk winds. The model of Blandford & Payne [74] treats the disk accretion rate as a constant which implies that the mass of the disk carried away by the wind is unimportant. The only velocity in the self-similar problem is the Kepler speed of the disk. Therefore, one anticipates that the various velocities in the problem scale as $v_A \propto c_s \propto v_r \propto v_\infty \propto v_K$ where one has the Alfvén, sound, radial inflow, terminal wind speed, and Kepler speed all being proportional to one another. Now, the hydrostatic balance condition for thin disk gives $H(r)/r = c_s/v_K$. Therefore, the self-similar scaling $c_s \propto v_K$ implies that $H \propto r$; the disk is wedge-like in its spatial structure. This also implies that the disk temperature follows the virial scaling $T \propto r^{-1}$. The density scaling for the disk follows from the definition of the disk accretion rate, $\dot{M}_a = 2\pi(2H\rho)v_r.r$, which given the scaling of the radial inflow velocity $v_r \propto v_K$ and the disk scale height relation implies that $\rho \propto r^{-3/2}$. The wind mass loss rate in the wind follows since the mass loss per unit area along the surface of the disk is $d\dot{M}_w/dA = \rho_o v_(w,o) \propto r_o^{-2}$, which imples that $M_w(r_o) \propto lnr_o$.

Next, note that the scaling of the disk Alfvén speed $v_A \propto v_K$, together with the density implies a particular scaling of the disk poloidal field, $B_p \propto r^{-5/4}$. In the BP model, the toroidal field on the disk should therefore scale as $B_\phi/B_p = const$, so that $B_\phi \propto r^{-5/4}$. This presents a bit of a dilema however because the lowest energy toroidal field would be expected to be a force-free condition which has a different scaling $B_\phi \propto r^{-1}$. The Alfvén surface in this model is then $v_\infty/v_K \propto r_A/r_o = const$; ie, a cone. Finally, given the scaling for the disk magnetic field, we can now calculate the mass load of the wind; $k_o \propto r_o^{-3/4}$.

What properties does a self-similar, collimated flow have? In a self-similar outflow with cylindrical asymptotics, and for a wind with a (spherical) density profile (where R is the spherical radius) $\rho \propto r^{-q}$, then the Alfvén radius scales as (in cylindrical radius) $r_A/r_o = [(4-2q)/(3-2q)]^{-1/2}$ [78]. For flow that is collimated to radial cylinders at infinity, the axial current scales as $r^{(1-q)/2}$ ([80]). It turns out that the hoop stress can collimate such a flow only if $q < 1$. Specific solutions can be constructed which are constrainted to collimate to a cylindrical radius r_1 subject to the power law density profile characterized by the value of q. As an example, for q=0.75 and $r_1/r_o = 2.86$, the Alfvén surface is found to occur at the radius $ir_A/r_o = 2.41$. The asymptotic velocities for these solutions are too small however, to account for observed jets. With the parameters above, $v_\infty/v_{K,o} \simeq$ a few 0.1. The Alfvén speed in the toroidal field is much larger than in the poloidal component however, with $v_{A,\phi}/v_{A,p} >> 1$. These results define an outflow that is driven primarily by a magnetic pressure gradient primarily in the toroidal component of the field. This can be thought of as a coiled, compressed spring that pops vertically upwards, pushing matter up the outflow axis (as in the simulations of Uchida & Shibata [82]).

Jets need not be self-similar structures however, and it is perhaps more natural to think of them as minimum energy configurations instead. We have seen above that for the magnetic configuration in which the toroidal field scales as $B_\phi \propto r_o^{-1}$, the current intensity is finite everywhere. The BP self-similar solution leads to diverging currents which corresponds to a higher energy state for the magnetic configuration. The disk-wind solutions elucidated by Pelletier & Pudritz [51] were designed to characterize non self-similar, but minimum energy-state jets. To derive this solution, we first write down the general Grad-Shafranov (GS) equation for stationary, axisymmetric flow, for the surfaces of magnetic flux $a(r,z)$ in the flow. Magnetic field lines are restricted to surfaces of constant magnetic flux,

$a(r,z) = const$, where the the poloidal magnetic field follows from the relation $\mathbf{B_p} = (1/r)\nabla(a)\times\hat{\phi}$. The GS equation can be written in a highly interesting form:

$$\frac{r^4}{m^2}(\nabla . \frac{m^2-1}{r^2}\nabla a) = \lambda(a)\bar{\eta}(a)a \tag{3.22}$$

where the function $\bar{\eta}(a) \simeq const$ and the function

$$\lambda(a) \equiv \frac{\Omega_o^2 r_A^2}{v_A^2} c_A = \frac{4\pi\rho_A(a)\Omega_o^2 r_A^6}{a^2}\left(\frac{dlnr_A}{dlna}\right)^2 \tag{3.23}$$

is a constant on a surface of constant magnetic flux and depends upon the density at the Alfvén point, ρ_A. Solving this last relation for the Alfvén radius, we see that $r_A \propto \lambda^{1/6}$ which is such a weak dependence that solutions with $\lambda = const$ were sought ([51]).

The disk in this picture imposes an important set of boundary conditions on the GS equation that include the value of the magnetic flux function across its surface; $a(r,z) = a_o(r_o, z_o)$. Without loss of generality one may assume that the flux takes on a power-law form on the disk; $a_o \propto r_o^{3/2\alpha}$. Using the Ansatz that $\lambda = const$, the preceeding equations show that the Alfvén surface takes the form $r_A/r_o \propto a^{2-\alpha} \propto r_o^{3/\alpha - 3/2}$ while the current takes the form $I(r,z) \propto a^{(\alpha/3)-1}$. The minimum energy state for the current arises from the solutions with $\alpha = 3$, for which $I = const$, $B_p \propto r_o^{-3/2}$, and the Alfvén surface behaves as $r_A/r_o \propto r_o^{-1/2}$. The terminal speed in this solution scales as $v_\infty \propto r_o^{-1}$. Finally, the mass loss rate in the wind for the PP92 solution is $\dot{M}_w \propto [(r_o/r_i) - 1]$, where r_i is the inner edge of the disk and the mass loading of the wind scales as $k \propto r_o^{-1/2}$. This mass loading is therefore a less steeply raked function of disk radius than in the BP self-similar case (wherein $k \propto r_o^{-3/4}$), which in turn suggests that the BP outflow may be more easily collimated than the PP92 outflow. (The BP solution is obtained for the choice $\alpha = 2$ for which $I \propto r_o^{-1/4}$ and $r_A/r_o = const$). We shall compare 2D time-dependent simulations of the BP with the PP92 boundary conditions in §4.1.

3.4 Accretion-Ejection Structures

The initiation of a disk wind may be different than occurs for winds from magnetized stars. For the latter, a star has a corona that is sufficiently well pressurized so as to help drive the magnetized wind. For disk winds however, a corona is not required as long as the field lines that emerge from the disk make an angle $\theta_o \leq 60^o$ ([74]). In this eventuality, it is the upper levels of the disk rather than the corona that is the mass source for the wind. The launch condition is found by applying Bernoulli theorem (equation 3.14) at the footpoint of a field line on the disk surface and comparing the change in the effective gravitational potential with the change in kinetic energy of a particle as it is moved an infinitesimal amount outward along the field line; $tan(\theta_o) = \delta z/\delta r \leq \sqrt{3}$ ([74]).

How is material launched from the disk in this cold, centrifugally driven wind picture? Without a corona, material from some height above the disk midplane must move upwards and eventually be accelerated outwards in a jet. Therefore, there must be a direct link between the physics of mangetized disks, and the origin of outflows - hence the idea of an "accretion-ejection" structure.

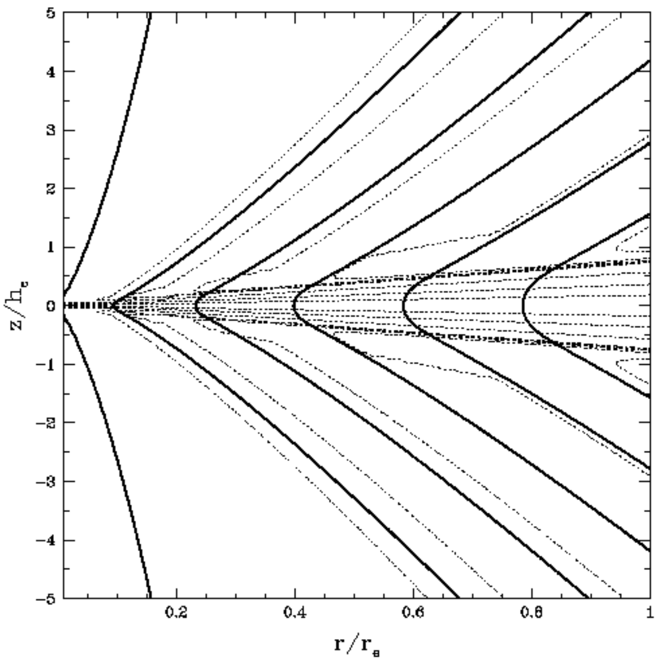

Fig. 3. Field lines (bold) and streamlines (dotted) of a self-similar accretion-ejection structure. Model parameters are $\epsilon = 0.1$, $\alpha_m = 1$, and ejection efficiency $\zeta = 0.004$ from Ferriera [84]. Courtesy of Jonathan Ferriera.

In order to see why this happens, let us follow a field line from the midplane of the disk out through its surface and then to large distances in a collimated outflow (see Figure 2, or 3). At the disk mid-plane, the poloidal field must be perpendicular to it ($B_r = 0$). If this were not so, there would be a singular current sheet on the mid-plane that would be unstable and would rapidly heat the disk until the current is dissipated. As one follows the field line from the mid-plane, it curves away from the rotation axis (convex) which is a consequence of the dragging of the field due to the inward accretion flow (see §2.7) which, as we have seen, is determined by the value of the magnetic Prandtl number. For a collimated flow to exist, this field line must begin to curve back towards the rotation axis (concave) of the system somewhere near the surface of the disk. Thus, the field changes its curvature from convex to concave as it traces through the disk. The magnetic tension associated with this curved field line exerts a pinch force down on the disk, compressing it at all heights (denoted by z_{curv}) below which the field-line curvature is convex. Above z_{curv} however, the (concave) curvature of the field exerts a tension force upwards, pushing the material slightly away from the disk mid-plane. It is this type of pressure imbalance which feeds gas in the upper layers of a disk into a cold disk wind ([83], [84]).

The formal expression of this physical picture is obtained from the condition of vertical hydrostatic balance ([83], [84]);

$$\frac{\partial P}{\partial z} = -\rho \Omega_K^2 z + F_z \tag{3.24}$$

where the vertical component of the Lorentz force is $F_z = J_r B_\phi - J_\phi B_r$. A deviation from this equilibrium solution will lead to matter either falling onto the disk mid-plane, or being lifted off the disk by a slight excees in pressure. The vertical profile of the radial current J_r thus plays a central role since a decrease of this current with height leads to a reversal of the direction of this force component.

The initiation of the outflow in the upper part of the disk above z_{curv} can be gleaned from the detailed angular momentum balance equation. The toroidal component of the Lorentz force on material rotating in the disk is $F_\phi = J_z B_r - J_r B_z$. One can see that as the radial current falls with height (z) in the disk, this component of the Lorentz force component also changes sign. Below the height z_{curv}, this force opposes the gas motion slowing it down slightly below Keplerian value and thereby causing it to fall to a slightly smaller disk radius; ie. accretion is affected by the magnetic torque. At heights in the disk $z > z_{curv}$ however, the force accelerates the gas slightly. It is this magnetic acceleration and upward direction of the force that gets the upper layers of the disk moving, eventually to become a cold, centrifugally driven disk wind. These types of models employ six disk parameters only four of which are independent ([84]): the disk profile $\epsilon \equiv h(r)/r$; the magnetic Reynold's number $Re_m = r v_r/\eta_T$; the strength of the magnetic turbulence $\alpha_m = \eta_T / v_A h$, which taken together, define the magnetic Prandtl number discussed in §2.7; the disk magnetic field strength $\mu = B^2/4\pi P_{gas}$; the "ejection index" $\zeta = dln\dot{M}_a/dlnr$ which describes the radial accretion flow and measures how much mass is ejected from each radius of the disk (akin to the mass loading); and finally, the vertical current profile $\Gamma \equiv (r[\partial\Omega/\partial r]B_r/J_r[\partial\eta_{T,\phi}/\partial z])|_{z=0}$ that controls the vertical force balance and the details of mass acceleration from the surface layers of the disk. Self-consistent flow solutions that evolve through the 3 critical points in the flow have been found which give a good correspondence with observed jets. The parameter ranges giving rise to these solutions are: $Re_m \simeq \epsilon^{-1}$, with $0.005 \leq \zeta \leq 0.08$; $0.0005 < \epsilon \leq 0.1$; and $0.1 < \alpha_m \leq 1$. Figure 3 gives a side view of a solution which shows both the magnetic field lines and particle trajectories in the disk and wind, for $\epsilon = 0.1$, $\alpha_m = 1$, and an accretion efficiency of $\zeta = 0.004$. While the previous solutions pertain to disks with purely magnetic torques, self-similar solutions that include viscous disk torques have also been found ([85]).

The assumption that disk winds get a cold start may not be entirely general since there are mechanisms for pumping energy into a disk corona. Extrapolating from what is observed in solar physics (§2.7), the expectation is that loops of magnetic flux as well as a flux of Alfvén waves propagate into the upper reaches of the disk atmosphere and deposit the energy released by accretion, there. Global simulations (in vertical scale) [64] of the MRI instability in accretion disks show that waves propagate into the upper reaches of disk, steepen, and then undergo strong shocks wherein their energy is converted into heat. These shocks occur at Mach numbers > 2. The simulations are highly time-dependent but in some cases they settle down into a disk-coronal structure in which the disk is weakly magnetized below two pressure scale heights (with $\beta = P_{gas}/(B^2/8\pi) \simeq 50$) and the corona is strongly magnetized above ($\beta \simeq 0.1$).

A resonant coupling picture for pumping Alfvén wave power into the disk corona has also been proposed [86], [87]. The resonant coupling of the MRI instability with Rossby vortices that are located at the co-rotation radius of the disk leads to the extraction of considerable gravitational binding energy interior to the co-rotation radius and its transmission into the corona by a flux of torsional Alfvén waves. Both of the above mechanisms suggest that there may be a much wider class of solutions for "accretion-ejection" structures in which accretion disk coronae, rather than the upper reaches of the disk, are the launch pads for disk winds.

Finally, a class of inflow-outflow solutions has been found that may combine gravitational collapse with accretion-ejection [88]. In these solutions, the region around a protostar is divided into three regions; a jet, an infalling envelope, and a circulation region in which matter rains down towards the central region and is reflected outwards again from a pressure gradient near the central region. This circulation region is interpreted as being the molecular outflow which is predicted not to arise not from the entrainment of surrounding molecular material by a fast moving jet, but by a separate hydrodynamic circulation flow in its own right. These solutions have a quadropolar symmetry with jets moving up the axes, and a ratio of wind outflow to accretion of the correct order; $\dot{M}_a/\dot{M}_w \simeq 0.1$.

3.5 Disk - Magnetosphere Coupling

For typical conditions in TTSs disks, accretion rates are low enough that a stellar magnetosphere rooted to the central star truncates the disk at an inner radius. The magnetopause radius of a dipole field interacting with an accretion disk has the well known scaling $R_{mag} \propto \mu^{4/7} \dot{M}_a^{-2/7}$, which is several stellar radii for typical TTS magnetic fields (here μ is the magnetic dipole moment of the star) and accretion rates. The interaction of this magnetosphere with the disk has been extensively analyzed by Shu and his collaborators (eg. [14]), and reviewed in this volume (see Calvet's, and Hartmann's contributions). The stress of an inner disk that is not exactly spinning at the rate of the central star should pump energy into the dipole field and open it up into an open structure [89]. This would drive a disk wind from a single annulus on the disk; its inner edge. This wind has most of its density collimated along the rotation axis of the outflow, and exerts a wide-angle outflow component as well. As we shall see in §4.1, disk winds can also have this feature.

It is interesting to apply this analysis to FU Ori systems where the accretion rate is four orders of magnitude greater than in the TTS stage. The scaling above then suggests that the magnetosphere will most likely be totally crushed to the stellar surface under these conditions and that the accretion disk will butt against the stellar surface [52]. These systems are still observed to have strong jets and outflows however. This is a clear indication that disk winds must be active in the FU Ori stage.

4 Numerical Simulations

The necessity of using excellent MHD codes to explore the physics of magnetized disks and jets is self-evident when one has such analytically intractable equations as the Grad-Shafranov equation to solve. The fact that jets are also highly episodic is yet another reason why time-dependent simulations of astrophysical MHD have rapidly become an essential research tool in the field.

The simulations have given important insights into how jets are launched and collimated, as well as into the coupling between jets and physical processes in the underlying disk such as the MRI instability. The published simulations mirror these two types of questions: i) *MHD disks as boundary conditions*, the underlying accretion disk remains constant and provides fixed boundary conditions for the outflow simulation, whereas; ii) *global simulations* , include both the dynamics of the disk and its jet. While the latter approach attempts to solve the entire accretion-ejection problem in one huge simulation, the rich variety of physical processes involved has given great importance to strategy (i) as well. We examine these in turn.

4.1 2D Simulations: Jets from Stationary Keplerian Disks

Several groups have exploited this approach including [90], [91], [92], [93], [94], [95], [96], [97]. The published simulations differ in their assumed initial conditions, such as the magnetic field distribution on the disk, the plasma β ($\equiv P_{\rm gas}/P_{\rm mag}$) above the disk surfaces, the state of the initial disk corona, and the handling of the gravity of the central star. Broadly speaking however, all of the existing calculations show that winds from accretion disks can indeed be launched and accelerated, much along the lines suggested by the theory presented above. This is reassuring and emphasizes the robustness of the theoretical model discussed in the previous section.

Many groups (including ours) employ the ZEUS 2-D code to study the origin and collimation of disk winds. This code is arguably the best documented and utilized MHD code in the literature (Stone & Norman [98]). It is an explicit, finite difference code that runs on a staggered grid. The evolution of the magnetic field is followed by the method of constrained transport [99]. In this approach, if $\nabla.\mathbf{B} = 0$ holds for the initial magnetic configuration, then it remains so for all later times to machine accuracy. The obvious way of securing this is to use an intial vector potential $\mathbf{A}(\mathbf{r}, \mathbf{z}, \mathbf{t} = \mathbf{0})$ that describes the desired initial magnetic field.

I will for illustrative purposes, first focus the discussion on the approach we have taken, as in [91], [92], [93], and [94] and documented in Ouyed & Pudritz [92]. The accretion disk in these papers is taken to be initially surrounded by a polytropic corona ($\gamma = 5/3$) that is in hydrostatic balance with the central object. The accretion disk at the base of the corona is given a density profile which it maintains at all times since the disk boundary conditions are applied to the "ghost zones" and are not part of the computational domain. It is chosen so that the disk surface is in pressure balance with the corona above it (ie. $\rho \propto r_o^{-3/2}$ for a $\gamma = 5/3$ model - as in BP). This hydrostatic state has a simple analytic solution which was used as the initial state for all of our simulations. We tested our numerical methods by ensuring that this eqilibrium state could be maintained for arbitrary amounts of machine time. We always use an unsoftened gravitational potential from the central object. The corona is ultimately swept away by the disk wind in all of these simulations so that the mass source for our jets becomes dominated by the material injected from the fixed disk below.

The initial magnetic configurations in our studies are chosen so that no Lorentz force is exerted on the initial (non-rotating) hydrostatic corona described above; more specifically, we used initial current-free configurations $\mathbf{J} = 0$ in the computational domain. The initial vector potential is subject to the boundary condition on the disk that the poloidal field on the disk surface $(r_o, 0)$ has a power-law form $B_z(r_o, 0) = b r_o^{\mu-1}$. The solution for $\mu = 0$ is analytic and is the so-called "potential" configuration which we used in many of our papers. This initial field configuration is shown in the upper left hand panel of Figure 4.

Recent work by Pudritz, Rogers, & Ouyed (2003, PRO [100]) is designed to simulate 2D disk winds from a greater variety of magnetized disks. One may accomodate other initial magnetic configurations by using a Hankel transform technique to solve for the initial vector potential that is subject to these constraints. In particular, we have now done simulations for an initial BP model ($\mu = -1/4$), PP92 ($\mu = -1/2$), and a yet more steeply declining magnetic field such as $\mu = -3/4$. These intial configurations are plotted out in the left panels of Figure 4. We also have simulated jets in the case of an initially uniform vertical field because of its unfavourable opening angle for launching a wind at all radii. The disk has an inner edge at radius $r_{\rm i}$, inside of which no material is rotating, and a uniform, vertical field that is everywhere parallel to the disk rotation axis.

These simulations of thin disks require that we specify five physical quantities at all points of the disk surface at all times. There are the disk density $\rho(r_o)$; components of the vertical and toroidal magnetic field, $B_z(r_o)$ and $B_\phi(r_o)$; and velocity components in the disk, $v_z(r_o)$ and $v_\phi(r_o)$. The remaining field component $B_r(r_o)$ is determined by the solenoidal condition while the radial inflow speed through the disk $v_r(r_o) \simeq 0$ for all practical considerations since it is far smaller than the sound speed in a real disk. The model is described by five parameters, whose values describe conditions at $r_{\rm i}$. Three of these parameters describe the initial corona: $\beta_{\rm i}$ which is typically 1.0 (and which therefore falls with radius); the density jump across the corona/disk boundary η_i which is typically 100; and ratio of the Keplerian to thermal energy density δ_i. Two additional parameters describe the disk physics. The important one is the injection speed $v_{\rm inj}$ of the material from the disk into the base of the corona. We scale the injection speed with the local Keplerian velocity at each radius of the disk where typically $v_{\rm inj} = 10^{-3} v_K$ at any point on the disk. This scaling and that of the magnetic field fixes the all-important mass loading at the footpoint of each field line on the disk;

$$k(r_o) = \rho_o v_{p,o}/B_{p,o} \propto r_o^{-3/2} r_o^{-1/2}/r_o^{-1+\mu} \propto r_o^{-1-\mu} \tag{4.1}$$

The second parameter, μ_i, which scales the toroidal field in the disk $B_\phi = \mu_i/r_o$ is unimportant. Even if it is set to zero there is little change in the results of the simulations since the disk will quickly produce a toroidal field in the computational domain just above the disk when its rotation is initiated.

We ran high resolution simulations in which (500×200) spatial zones were used to resolve a region $20 r_i$ in radius and $80 r_i$ in the z direction. Our simulations ran up to $400 t_{\rm i}$ (where $t_{\rm i}$ is the Kepler time for an orbit at the inner edge of the disk, $r_{\rm i}$). The standard parameter settings were

$$(\eta_i, \mu_i, v_{inj}, \delta_i, \beta_i) = (100.0, 1.0, 0.001, 100.0, 1.0) \tag{4.2}$$

The details of the outflow in the "potential" configuration ($\mu = 0$) are found in [91], [92]. The disk immediately begins to generate a centrifugally driven outflow that drives a bow shock through the corona. The highest velocity and densest material is found near to the rotation axis in agreement with the prediction of equation (3.15) and the observations shown in Figure 1, §2.1. In the final time frame at $t = 400$ (the bowshock clears the grid earlier), the flow is highly collimated. The magnetic configuration at this time is shown in the top right panel of Figure 4 where one sees that the field lines have been bent from an initial parabola like configuration into a state in which the field lines are almost parallel to the outflow axis in this computational domain. This panel of Figure 4 also shows the position of the Alfvén surface and a few FM points as well. The position of the Alfvén surface matches the theoretical prediction very well [92]. The toroidal field generated by the jet is responsible for collimating the outflow.

The outflow begins to collimate just beyond the Alfvén surface and is largely accomplished by the time that the FM surface is reached. The ratio of the toroidal to the poloidal field strength at the FM surface is between 2 - 3 for many field lines. We also find that the opening angles of field lines as they emerge from the disk and along which an outflow is driven, obey $\theta_o \leq 60^0$ again as predicted by steady state theory.

Outflows also occur in an initially uniform, vertical magnetic field configuration. This is possible because the pressure gradient $\partial(B_\phi^2/8\pi)/\partial r$ generated in the jet pushes the fields lines radially outwards above the disk surface thus allowing the wind to be accelerated and ejected. The gradient arises from the fact that the strongest toroidal magnetic field is generated in the inner region of the flow where the Kepler speed is the highest.

What systematic differences can be expected from jet models as the magnetic fields, or other physical boundary conditions, are varied. To what extent is the structure of the jet controlled by the physics of the accretion disk? This question is pursued by PRO [100] in a series of simulations in which the initial magnetic configurations are varied but which otherwise adopt the same initial conditions as OPS.

Figure 4 (from PRO) plots the magnetic field lines of both the initial states of each model (left panels) as well as the final states of simulations. In addition to the potential case, simulations of the Blandford-Payne, Pelletier-Pudritz, as well as an even more steeply raked initial magnetic configuration are shown. It is evident that the field lines in these right hand panels are progressively less collimated towards the axis suggestive of a wide angle flow at larger radii. Also marked on these field lines are the positions of the Alfvén surfaces for each configurations. The BP final states shows that the Alfvén surface is indeed nearly a cone as expected while the PP simulation qualitatively agrees with the expected scaling $r_A \propto r_o^{1/2}$ (see §3.3).

Figure 5 shows snapshots of the evolution of the density of the jet for

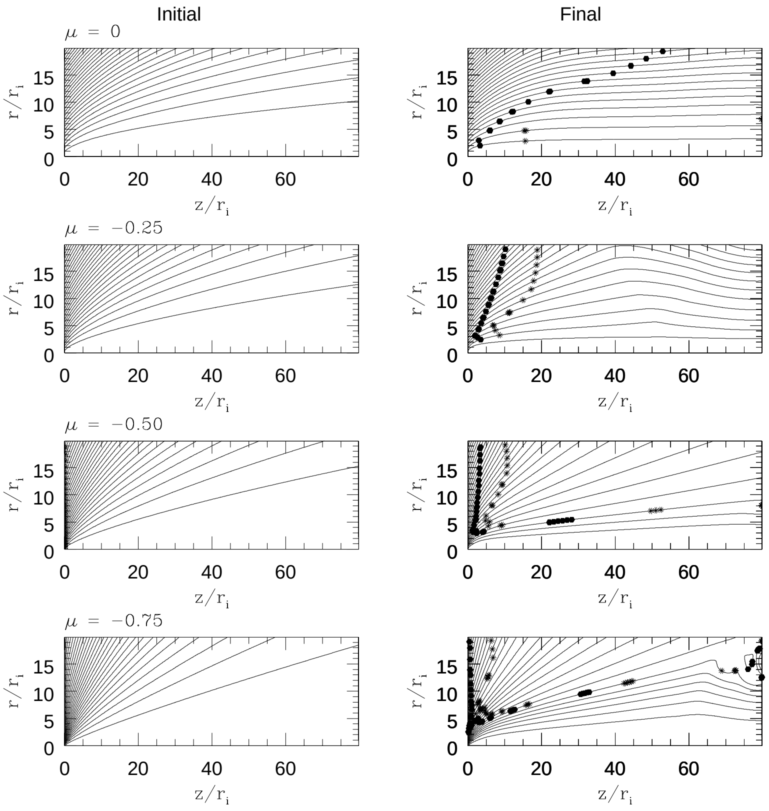

Fig. 4. Left panels: initial magnetic field configurations for winds with initial potential ($\mu = 0$), Blandford & Payne ($\mu = -0.25$), Pelletier & Pudritz ($\mu = -0.5$), and steeper ($\mu = -0.75$) configurations shown. Right panels: final magnetic field configurations (at t = 400) for each case, with Alfvén points (filled circles) and FM points (stars) marked. From PRO [100]. Note the more open magnetic - and stream line structures as the initial magnetic configuration (value of μ) changes.

the BP (left panels) and PP (right panels) models at 4 different times ($t = 60, 120, 200, 400$). In each case we see the jet driving a bow shock through the quiescent gas in the first frame. In the second frame the shock has just moved out of the grid. The densest gas in the jet is always well collimated and moving nearly parallel to the axis. Comparison with Figure 4 though shows that there is material that is moving outwards in a less collimated fashion, following the less well collimated field lines.

The poloidal jet velocities for these two simulations of BP and PP initial conditions are shown in Figures 6 and 7 respectively. The four frames shown

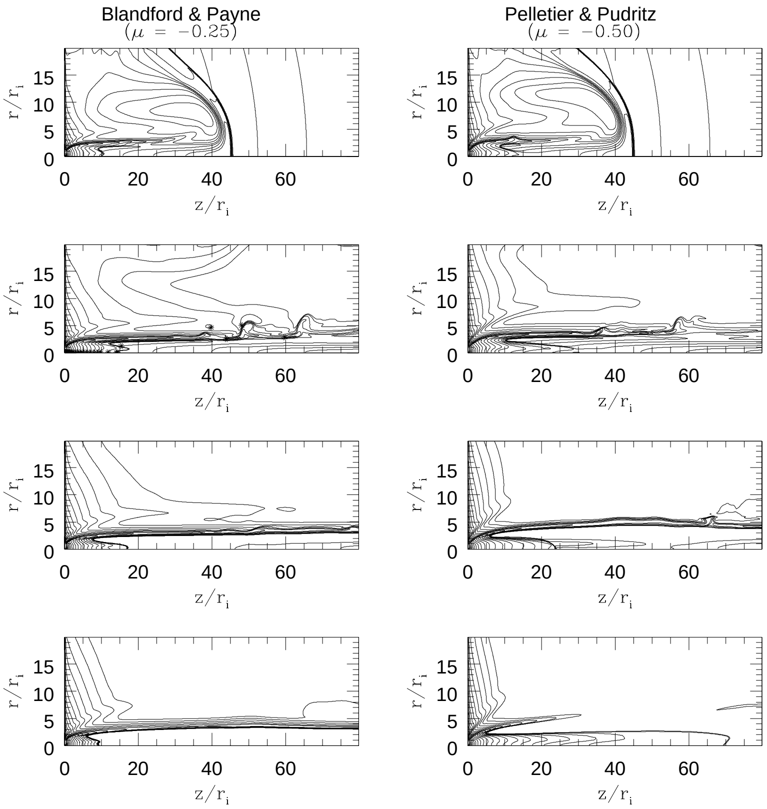

Fig. 5. Density structure of jets from Blandford-Payne (left panels), or Pelletier-Pudritz (right panels) initial conditions. Contours mark surfaces of constant density in the jet at four different times (t= 60, 120, 200, 400). Note the densest material moves along the jet axis. From PRO.

in each of these panels correspond to the 4 times shown in Figure 5. In both Figs. 6 and 7 we see that the highest velocity gas is the best collimated and occurs closest to the rotation axis. In both cases, the velocity falls off with radial distance, reflecting the fact that the footpoints of these field lines rotate more and more slowly as expected for Keplerian rotation. The high-speed well collimated gas grades continuosly into the lower-speed, less collimated flow at larger radial distance from the outflow axis. Finally, we see that the jet recollimates in each case, as was pointed out by BP and PP. These two figures bear strong relations to the observations shown in Figure 1. It is apparent that a wide-angle aspect to this outflow exists for disk winds - not only X-wind solutions [14].

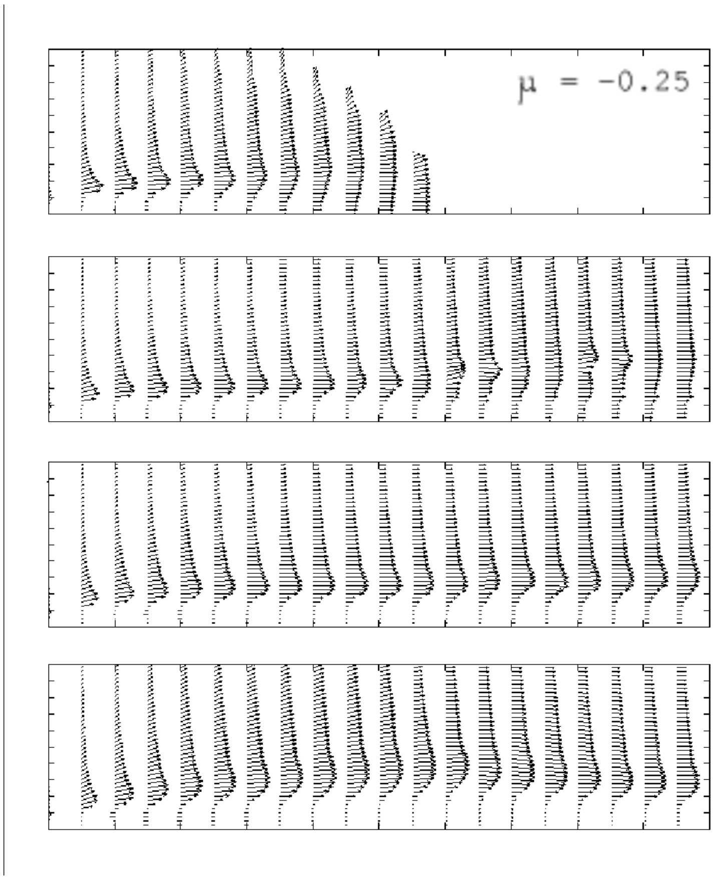

Fig. 6. Poloidal velocity field of a Blandford-Payne jet, shown at 4 different times as in Figure 5. Note that the highest velocities are nearest the outflow axis, and that the flow gently recollimates. From PRO.

These simulations of a variety of disk winds have all the attributes of jets suggested by the observations (see §2.1). There is no need to postulate that observed outflows have separate high speed cores and wide-angle disk winds that are produced by different mechanisms. Rather, it is a reflection of the physics of the jet launched from the disk, and on the distribution of magnetic flux across the surface of the disk. The degree of collimation of the field lines in these flows is probably controlled by their mass loading. In going from BP to PP models as an example, k increases from $k \propto r_o^{-3/4}$ to $k \propto r_o^{-1/2}$ which implies that it is harder for the toroidal field to collimate the increasingly mass-loaded outflow (equation 3.8 and discussion).

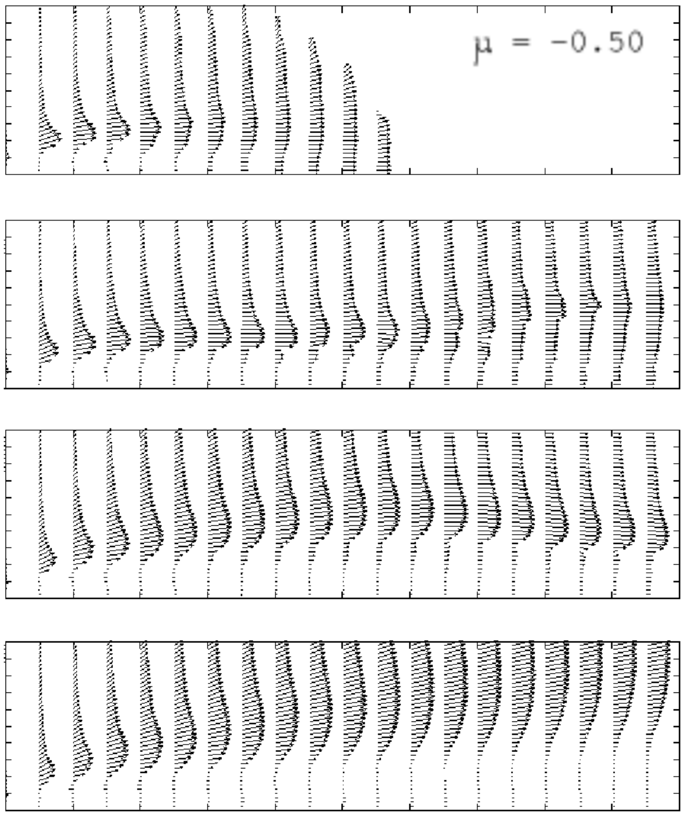

Fig. 7. Same as Figure 6 except showing the Pelletier-Pudritz jet. The flow is less well collimated while the highest speed material (which is also the densest) is closest to the outflow axis. This shows a wide-angle behaviour to the flow. From PRO.

The robustness of these results follows from the fact that simulations with very different initial conditions produce qualitatively the same picture. Thus Krasnopolsky et al. [97] set up fiducial models with a constant density disk; a poloidal magnetic flux distribution on the disk idential to PP ($\mu = -1/2$); and a mass flux density $\rho v_z \propto r_o^{3/2}$ which leads to a mass loading $k = const$ across the disk. An important difference in their boundary conditions is their injection of a thin, axial jet along the rotation axis chosen to mimic the possible production of a relativistic jet by a central spinning object. In [92] the coronal material that is initially in equilibrium along the rotation axis is squeezed outward by the jet when it is formed, which leaves a "hole" at the centre of their disk-wind. Once again however, collimation of the flow is observed. Also, the outflow is insensitive to the density or injection speed at the base of the wind as long as the mass flux is left unaffected.

Jets launched in the most extreme initial magnetic field geometry on the disk - a so-called split monopole configuration - have also been simulated [95]. The field lines in this configuration constitute a very steeply decreasing function of radius. In these simulations too, the densest gas has the highest speeds and is closest to the rotation axis. The field lines however do not collimate and some of the material does flow outwards radially.

It appears therefore that a common theme is established with all the disk-wind simulations. In all cases one sees the densest material moving at the highest speeds parallel to the axis, with lower density gas moving off in a less collimated way. This behaviour is also observed in the X-wind model - discussed in §3.5. It appears therefore that the X-wind is not a unique explanation of wide-angled outflows. Disk winds with appropriately falling field strengths can also do the job (see PRO for details).

Finally, how does the apparently universal, episodic behaviour of jets arise? There are indications that disk winds naturally do this. We have also discovered episodic jets in our simulations - found by sufficiently "starving" the acceleration zone of material from the disk [93], [94]. Episodic behaviour of jets can be initiated by sufficiently reducing the injection speed of material from the disk into its corona and thereby reducing the mass loading of field lines. These episodic states appear to be independent of the magnetic configuration that is employed (we find them for both uniform field and potential configurations), and they *never* become stationary. The region of knot generation is located at a distance of $z \simeq 5 - 7r_i$ from the central source, beyond the Alfvén surface.

Knots in 2D simulations are produced on a time scale that is expected for sausage instability, the so-called $m = 0$ mode. Our simulations [93] show that if $r_{\rm jet}$ is the radial size of the jet region, then the time scale for knot production at the generator region is, roughly $\tau_{\rm knot} \simeq r_{\rm jet}/v_{A,\phi}$. The knots are coherent structures that propagate down the length of the jet. The transition from episodic to stationary jets occurs for sufficiently well mass loaded field lines in any given magnetic configuration. The transition to episodic behaviour can be quantified by the value of the quantity $N \equiv B_\phi^2/8\pi\rho v_{\rm p}^2$. In general, stationary flows involve low values for N (high mass load), while episodic jets typically occur for higher values for N (low mass load) [94].

4.2 3D Simulations: Self-Regulatory Stability of Jets

One of the central challenges to the theory of jets is in accounting for their 3D stability. Why don't outflows that are dominated by toroidal field un-

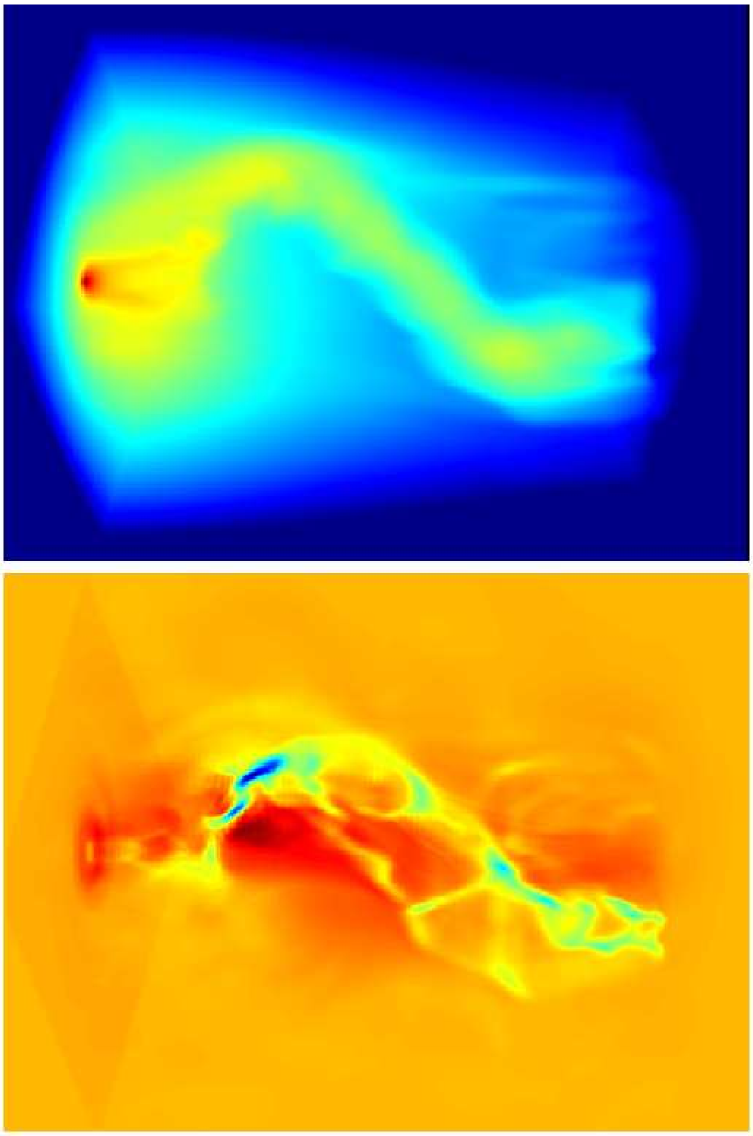

Fig. 8. A corkscrew jet from an accretion disk (shown on the left-hand side of each panel, in projection). Top frame is the column density through the jet, and the bottom frame is a measure of its compression. This jet survives because of the nonlinear saturation of KH instabilities, which prevent jet velocities from exceeding the Alfvén speed. From Ouyed, Clarke, and Pudritz [104].

dergo catastrophic kink mode instabilities that would tear them apart? While 3D computational studies of jet stability have been performed in the context of extragalactic radio jets [101] most of these simulations are done for jets that propagate from orifices. What about astrophysical jets that are produced by accretion disks?

The Kelvin-Helmholtz instability is one of the primary threats to the propagation of jets in 3D. There are several ways in which jets can survive this however. Linear instability analysis of magnetized jets showed that long wavelength kink modes (m=1) are stable for all wavelengths greater than the jet radius R (ie, for $kR \leq 1$) as long as the flows are sub-Alfvén (ie. $m_a \leq 1$) [102]. This was confirmed in 3D simulations of "equilibrium jets" - models with uniform density [101]. Analytic work also suggests that jets are increasingly stabilized at progressive larger scales as the fast magnetosonic Mach number becomes large. Finally, the cores of jets from accretion disks will have "backbones" of poloidal magnetic field that can resist kinks [103]. These arguments suggest that jets should be particularly vulnerable to instability in the regime of moderate super Alfvénic Mach numbers but with lower FM Mach numbers - that is in the region beyond the Alfvén surface but before the FM Mach numbers have gotten too large.

3D simulations of jets with boundary conditions identical to those in the 2D simulations of [93] (constant initial vertical field), were performed by Ouyed, Clarke, & Pudritz (2003, [104]). These simulations - although performed on a Cartesian rather than axisymmetric grid, run at lower resolution, and subject to symmetry breaking by the effective wobbling of the disk - were otherwise identical to [93]. During the early rather stable evolution of the jet until times $t \simeq 100$, the jet behaves much like its 2D counterpart undergoing sausage (m=0) modes but otherwise fairly stable. After this time, these modes merge together and the (m=4) mode symptomatic of the symmetry breaking appears. At the time t=160, the m=1 "kink" mode is strong and the jet appears to be severely stressed. However, the jet survives this and by t=200 to the end of the simulation at t=240, the jet settles down and runs in a stable way with a low amplitude m=1 perturbation. The body of the jet is displaced from the axis and winds around it in a stable "corksrew" morphology. This stable end-state is shown in Figure 8. The upper frame shows is a map of the jet column density while the lower frame maps the quantity $\nabla . \mathbf{v}$ which measures the compression of the jet. These jets survive growing instability and adopt a final state that is often seen in YSO jets. Why?

The nonlinear saturation of the jet's Kelvin-Helmholzt (KH) instability arises as a response to the buckling of the jet by the instability. The KH instability sets in when the jet becomes fairly super-Alfvénic as previous papers have suggested. This drives the m=1 mode which becomes predominant at t=160. This mode stretches and twists the poloidal magnetic field, thereby strengthening it through the tension force. Thus, energy drained from the kinetic energy by the instability bolsters the poloidal field, and thereby reduces the Alfveén Mach number m. The instability shuts itself off when the jet Alfvén Mach number is reduced to below unity, which kills the KH instability. Thus saturation occurs not because of a large reduction of the flow speed, but rather through the increase of the Alfvén velocity due the the increased poloidal field strength. These results are robust in that stabilization occurs for a variety of jet boundary conditions and initial perturbuations.

4.3 Global Simulations of Accretion-Ejection Structures

The first disk and wind numerical calculations were published by Uchida and Shibata [82]. These pioneering simulations were carried out for magnetized disks with sub-Keplerian rotation, designed to mimic the collapse of an initially more extended and slowly rotating object. Their models developed a rapid radial collapse in which the initially poloidal field threading the disk winds up due to the differential rotation of the collapsing disk. The vertical Alfvén speed being smaller than the free-fall collapse speed implies that a strong, vertical toroidal field pressure gradient $\partial B_z^2/\partial z$ must rapidly build up. The resulting vertical pressure gradient results in the transient ejection of coronal material above and below the disk as the spring uncoils (see also [105]). These outflows, while very suggestive, represent more transient responses to the initial state.

Stone and Norman [105] ran a series of ZEUS 2-D simulations for a uniform magnetic field threading a wedge-shaped disk of constant opening angle. Among their simulations was the case of a Kepler disk with an initially weak field. Due to the extremely strong channel instability arising from the MRI instability in 2D, the simulation discovered that the disk collapses very rapidly in the radial direction. without a strong toroidal field being formed (also [106]). These highly unstable channel flows arising from MRI instability in 2D become turbulent in 3D and the rate of outward angular momentum transport is considerably reduced (eg. [107]). This makes 3D simulations indispensible for this problem. More recent global simulations of the MRI instability in a torus threaded by a weak uniform, vertical initial field show that accretion flow, MRI instability, as well as mass ejection rapidly ensue [108]. Although the simulations are run only until t = 5, the relationship between mass accretion and outflow rates discussed earlier manages to establish itself. Here too, $\dot{M}_w/\dot{M}_a \simeq 0.1$!

We close with a return to the large picture of star formation in the Class 0 stage wherein collapse, disk accretion, and outflow are all simultaneously in play. Tomisaka [109] has attacked this problem with a subtle use of nested grids in order to gain the required large dynamical range. His simulations show that the collapse of an intially magnetized filament produces a magnetized disk that drives an outflow with many of the characteristics that we have cited here. Much more remains to be done in this fertile global numerical domain, particularly with the advent of adaptive mesh refinement codes.

5 Conclusion

These lectures have shown that the accretion-ejection mechanism for jets has an elegant simplicity. Astrophysical jets are inevitable because magnetic fields are inevitable in astrophysical plasmas. Whether these fields are dragged in from elsewhere, or generated in situ by the MRI instability, disks cannot help but becoming substantially magnetized. The MHD conservation laws then assure us that the torques that are exerted by such ordered fields upon their disks are extremely efficient in transporting angular momentum and gravitational binding energy in an ordered and well-collimated manner. The fact that jets are seen in black hole systems that have no central dipole magnetic fields, as well as in YSOs which do, suggests that it is their accretion disks rather than the central objects themselves that may be playing the central role in non-relativistic or mildly relativistic outflows.

Gravity is the prime mover in this model of jets. One of the most promising aspects of the disk wind model for jets is their prediction that it is the gravitational binding energy that is liberated due to accretion that ultimately powers jets in the vast majority of disk-jet systems. This provides a powerful unifying idea for all jets - their central source is largely irrelevant and only the depth of the gravitational potential that they imprint really matters. Many aspects of MHD jets including their stability and the presence of both collimated and wide-angle outflow sectors have also been confirmed in numerical experiments.

The richness of any scientific field is measured by the number of new and exciting ideas and questions that it generates. Jets are an efficient means of transporting angular momentum in a wide range of astrophysical systems. Nothing could be more fundamental to their evolution. By this measure, the study of astrophysical jets should enjoy a long and excellent future.

I am indebted to the organizers of this wonderful school for the invitation to participate and for their patience during the preparation of my written lectures. I enjoyed many conversations with the students of the school, as well as Vasily Beskin, Max Camenzind, Nuria Calvet, Lee Hartmann, Jean Heyvaerts, Francois Menard, Guy Pelletier, and Rachid Sunyaev. I sincerely thank my collaborators, postdocs, and students over the years - David Clarke, Ana Gomez de Castro, Arieh Königl, Sean Matt, Colin Norman, Guy Pelletier, Conrad Rogers, Jim Stone, and especially Rachid Ouyed - for their insights, hard work, and friendship. Special thanks to Sean Matt for useful comments on this manuscript. My research is supported through a grant from the Natural Sciences and Engineering Research Council of Canada.

References

[1] Reipurth, B., and Bally, J. 2001, ARA&A, 39, 403.

[2] Richer, J.S., Shepherd, D.S., Cabrit, S., Bachiller, R., & Churchwell, E. (2000) "Molecular outflows from young stellar objects", in Protostars and Planets IV, ed. V. Mannings, A. P. Boss, & S. S. Russell (Tucson: Univ. Arizona Press), 867.

[3] Mirabel, I. F. and Rodriguez, L. F. (1998), Nature, 392, 673

[4] Begelman, M. C., Blandford, R. D., and Rees, M. (1984), Rev. Mod. Phys., 56, 255.

[5] Balick, B., and Frank, A. 2002, ARA&A, 40, 439.

[6] Weisskopf, M.C. et al. 2000, ApJ, 536, L81.

[7] Königl, A., and Pudritz, R. E. (2000), "Disk Winds and the Accretion-Outflow Connection", in Protostars & Planets IV, V. Mannings, A.P. Boss, and S.S. Russell eds. Tucson: Univ. of Arizona Press), 759.

[8] Spruit, H. C. 1996, in NATO ASI Ser. C. 477, Evolutionary processes in binary stars, R. A. M. J. Wijers, M. B. Davies, and C. A. Tout, Dordrecht: Kluwer, 249

[9] Bachillor, R. 1996, ARA&A, 34, 111.

[10] Shepherd, D.S., and Churchwell, E. 1996, ApJ, 472, 225.

[11] Cabrit, S., and Bertout,C. (1992), A&A, 261, 274.

[12] Raga, A., and Cabrit, S. 1993, A&A, 278, 267.

[13] Masson, C. R., and Chernin, L. M. 1993, ApJ, 414, 230

[14] Shu, F. H., Najita, J., Shang, H., and Li, Z.-Y. (2000), "X-Winds: Theory and Observations", in Protostars and Planets IV, ed. V. Mannings, A. P. Boss, & S. S. Russell (Tucson: Univ. Arizona Press), 789

[15] Cabrit, S., Raga, A. C., and Gueth, F. 1997, in Herbig-Haro Flows and the Birth of Low Mass Stars, B. Reipurth and C. Bertout, Dordrecht: Kluwer, 163

[16] Lee, C-F, Mundy, L.G., Reipurth, B., Ostriker, E.C., and Stone, J.M. 2000, ApJ, 542, 925.

[17] Adams, F.C., Lada, C.J., and Shu, F.H. 1987, ApJ, 321, 788.

[18] André, P., Ward-Thompson, D., and Barsony, M. 1993, ApJ, 406, 122.

[19] Pudritz, R. E., Wilson, C. D., Carlstrom, J. E., Lay, O. P., Hills, R. E., and Ward-Thompson, D. 1996, ApJ, 470, L123.

[20] Looney, L.W., Mundy, L.G., and Welch, W.J. (2000), ApJ, 529, 477.

[21] Chandler, C.J., and Richer, J.S. (1999), "Observations of circumstellar discs and jets", in Astrophysical Discs, ASP Conference Series Vol. 160, J.A. Sellwood, and J. Goodman, eds. (ASP, San Francisco), 91.

[22] Dougados, C., Cabrit, S., Lavalley, C., and Ménard, F. 2000, A&A, 357, L61.

[23] Bacciotti, F., Ray, T.P., Mundt, R., Eilöffel, J., Solf, J., and Camenzind, M. (2000), 537, L49.

[24] Kwan, J., and Tademaru, E. 1988, ApJ, 332, L41.

[25] Bacciotti, F., Ray, T.P., Mundt, R., Eilöffel, J., and Solf, J. (2002), ApJ, 576, 222.

[26] Burrows, C. J., et al. 1996, ApJ, 473, 437

[27] Hartmann, L., & Kenyon, S. J. 1996, ARAA, 34, 207

[28] Beckwith, S.V.W., Sargent, A.I., Chini, R.S., and Güsten, R. 1990, AJ, 99, 924.

[29] André, P., and Montmarle, T. 1994, ApJ, 420, 837.

[30] Lada, C.J., Young, E.T., and Greene, T.P. 1993, ApJ, 408, 471.

[31] Gomez, M., Whitney, B. A., and Kenyon, S. J. 1997, AJ, 114, 1138.

[32] Cabrit, S., and André, P. 1991, ApJ, 379, L25

[33] Hartmann, L., and Calvet, N. 1995, AJ, 109, 1846

[34] Calvet, N. 1997, "Properties of the Winds of T-Tauri Stars", in Herbig-Haro Flows and the Birth of Low Mass Stars, IAU Symposium 182, B. Reipurth, and C. Bertout eds. (Dordrecht: Kluwer), 417.

[35] Calvet, N., Hartmann, L., and Kenyon, S. J. 1993, ApJ, 402, 623

[36] Crutcher, R.M. 1999, ApJ, 520, 706.

[37] Greaves, J. S., Murray, A. G., and Holland, W. S. 1994, MNRAS, 284, L19

[38] Schleuning, D. A. 1998, ApJ, 493, 811.

[39] Matthews, B., and Wilson, C.D. 2000, ApJ, 531, 868.

[40] Fiege, J., and Pudritz, R.E. 2000a, MNRAS, 311, 85.

[41] Fiege, J., and Pudritz, R.E. 2000b, ApJ, 544, 830.

[42] Ray, T., Muxlow, T. W. B., Axon, D. J., Brown, A., Corcoran, D., Dyson, J., and Mundt, R. 1997, Nature, 385, 415

[43] Thum, C., and Morris, D. 1999, A&A, 344, 923.

[44] Levy, E. H., and Sonnett, C. P. 1978, "Meteorite magnetism and early solar system magnetic fields", in Protostars & Planets, T. Gehrels ed. (Tucson: Univ. of Arizona Press), p. 516.

[45] Feigelson, E.D., and Montmerle, T. 1999, ARA&A, 37, 363.

[46] Glassgold, A.E., Feigelson, E.D., and Montmerle, T. 2000, "Effects of Energetic Radiation in Young Stellar Objects", in Protostars and Planets IV, ed. V. Mannings, A. P. Boss, & S. S. Russell (Tucson: Univ. Arizona Press), 429,

[47] Foster, P.N., and Chevalier, R.A. 1993, ApJ, 416, 303.

[48] Reid, M.A., Pudritz, R.E., and Wadsley, J. 2002, ApJ, 570, 231.

[49] Bontemps, S., André, P., Terebey, S., and Cabrit, S. 1996, A&A, 311, 858

[50] Pudritz, R. E., and Norman, C. A. 1986, ApJ, 301, 571.

[51] Pelletier, G., and Pudritz, R. E. 1992, ApJ, 394, 117

[52] Hartmann, L. 1997, in Herbig-Haro Flows and the Birth of Low Mass Stars, B. Reipurth and C. Bertout eds. (Dordrecht: Kluwer), 391

[53] van Paradijs, J., and White, N. 1995, ApJ, 447, L33.

[54] Mirabel, I.F., and Rodriquez, L.F. 1994, Nature, 371, 46.

[55] Miyoshi, M. et al. 1995, Nature, 373, 127.

[56] Herrnstein, J.R. et al. 1997, ApJ, 475, L17.

[57] Blandford, R.D. 1999, "Relativistic Accretion", in Astrophysical Discs, ASP Conference Series Vol. 160, J.A. Sellwood, and J. Goodman, eds. (ASP, San Francisco), 265.

[58] Narayan, R., and Yi, I. 1994, ApJ, 428, L13.

[59] Blandford, R.D., and Begelman, M.C. 1999, MNRAS, 303, L1.

[60] Sakurai, T. 1985, A&A, 152, 121.

[61] Aschwanden, M.J. et al. 2000, ApJ, 535, 1047.

[62] Chandrasekhar, S. 1961, Hydrodynamic and hydromagnetic stability. (Clarendon: Oxford).

[63] Balbus, S. A., and Hawley, J. F. 1991, ApJ, 376, 214

[64] Miller, K.A., and Stone, J.M. 2000, ApJ, 534, 398.

[65] Lubow, S. H., Papaloizou, J. C. B., and Pringle, J. 1994, MNRAS, 267, 235.

[66] Tout, C. A., and Pringle, J. E. 1996, MNRAS, 281, 219.

[67] Brandenburg, A., Nordlund, A, Stein, R.F., and Torkelsson, U. 1995, ApJ, 446, 741.

[68] Curry, C., Pudritz, R. E., and Sutherland, P. G. 1994, ApJ, 434, 206

[69] Armitage, P.J. 1998, ApJ, 501, L189.

[70] Gammie, C. F. 1996, ApJ, 457, 355.

[71] Matsumura, S., and Pudritz, R.E. 2003, ApJ, submitted.
[72] Mestel, L. 1968, MNRAS, 138, 359.
[73] Weber, E. J., and Davis, L. 1967, ApJ, 148, 217.
[74] Blandford, R. D., and Payne, D. G. 1982, MNRAS, 199, 883
[75] Michel, F. C. 1969, ApJ, 158, 727
[76] Heinemann, M., and Olbert, S. 1978, J. Geophys. Res., 83, 2457.
[77] Tsinganos, K., and Trussoni, E. 1990, A&A, 231, 270.
[78] Li, Z.-Y. 1995, ApJ, 444, 848.
[79] Königl, A. 1989, ApJ, 342, 208.
[80] Ostriker, E. 1998, ApJ, 486, 291.
[81] Heyvaerts, J., and Norman, C. A. 1989, ApJ, 347, 1055.
[82] Uchida, Y., and Shibata, K. 1985, PASJ, 37, 31.
[83] Ferreira, J., and Pelletier, G. 1995, A&A, 295, 807.
[84] Ferreira, J. 1997, A&A, 319, 340.
[85] Casse, F., and Ferreira, J. 2000, A&A, 353, 1115.
[86] Tagger, M., and Pellat, R. 1999, A&A, 349, 1003.
[87] Varniere, P., and Tagger, M. 2002, A&A, 394, 329.
[88] Lery, T., Henriksen, R.N., Fiege, J.D., Ray, T.P, Frank, A., and Bacciotti, F. 2002, A&A, 387, 187.
[89] Goodson, A. P., Winglee, R. M., and Böhm, K-.H. 1997, ApJ, 489, 199.
[90] Ustyugova, G.V. et al., 1998, ApJ, 500, 703.
[91] Ouyed, R., Pudritz, R. E., and Stone, J. M. 1997, Nature, 385, 409.
[92] Ouyed, R., and Pudritz, R. E. 1997a, ApJ, 482, 712.
[93] Ouyed, R., and Pudritz, R. E. 1997b, ApJ, 484, 794.
[94] Ouyed, R. and Pudritz, R. E. 1999, MNRAS, 309, 233.
[95] Romanova, M. M., Ustyugova, G. V., Koldoba, A.V., Chechetkin, V.M., and Lovelace, R. V. 1997, ApJ, 482, 708.
[96] Meier, D.L., Eddington, S., Godon, P., Payne, D.G., and Lind, K.R. 1997, Nature, 388, 350.
[97] Krasnopolsky, R., Li, Z-Y, and Blandford, R.D. 1999, ApJ, 526, 631.
[98] Stone, J.M., and Norman, M.L. 1992, ApJS, 80, 753
[99] Evans, C.R., and Hawley, J.F. 1988, ApJ, 332, 659.
[100] Pudritz, R.E., Rogers, R., and Ouyed, R. 2003 , in preparation (PRO).
[101] Hardee, P.E., and Rosen, A. 1999, ApJ, 524, 650.
[102] Ray, T.P. 1981, MNRAS, 196, 195.
[103] Appl, S., and Camenzind, M. 1992, A&A, 256, 354.
[104] Ouyed, R., Clarke, D.A., and Pudritz, R.E. 2003, ApJ, 582, 292.
[105] Stone, J.M., and Norman, M.L. 1994, ApJ, 433, 746.
[106] Bell, A.R., and Lucek, S.G. 1995, MNRAS, 277, 1327.
[107] Goodman, J., and Xu, ApJ, 432, 213.
[108] Kudoh, T., Matsumoto, R., and Shibata, K. 2002, PASJ, 54, 121.
[109] Tomisaka, K. 1998, ApJ, 502, L163.